Interleukin-2 signals converge in a lymphoid-dendritic cell pathway that promotes anticancer immunity.

Raeber, Miro E ; Rosalia, Rodney A ; Schmid, Dominic ; Karakus, Ufuk ; Boyman, Onur

Abstract: Tumor-infiltrating dendritic cells (DCs) correlate with effective anticancer immunity and improved responsiveness to anti-PD-1 checkpoint immunotherapy. However, the drivers of DC expansion and intratumoral accumulation are ill-defined. We found that interleukin-2 (IL-2) stimulated DC formation through innate and adaptive lymphoid cells in mice and humans, and this increase in DCs improved anticancer immunity. Administration of IL-2 to humans within a clinical trial and of IL-2 receptor (IL-2R)-biased IL-2 to mice resulted in pronounced expansion of type 1 DCs, including migratory and cross-presenting subsets, and type 2 DCs, although neither DC precursors nor mature DCs had functional IL-2Rs. In mechanistic studies, IL-2 signals stimulated innate lymphoid cells, natural killer cells, and T cells to synthesize the cytokines FLT3L, CSF-2, and TNF. These cytokines redundantly caused DC expansion and activation, which resulted in improved antigen processing and correlated with favorable anticancer responses in mice and patients. Thus, IL-2 immunotherapy-mediated stimulation of DCs contributes to anticancer immunity by rendering tumors more immunogenic.

DOI: https://doi.org/10.1126/scitranslmed.aba5464

Title: Interleukin-2 signals converge in a lymphoid–dendritic cell pathway that promotes anti-cancer immunity

Authors: Miro E. Raeber[1], Rodney A. Rosalia[1], Dominic Schmid[1], Ufuk Karakus[1], and Onur Boyman[1,2,*]

Affiliations:

[1] Department of Immunology, University Hospital Zurich, CH-8091 Zurich, Switzerland

[2] Faculty of Medicine, University of Zurich, CH-8006 Zurich, Switzerland

*Correspondence: onur.boyman@uzh.ch (O.B.)

ABSTRACT

Tumor-infiltrating dendritic cells (DCs) correlate with effective anti-cancer immunity and improved responsiveness to anti-PD-1 checkpoint immunotherapy. However, the drivers of DC expansion and intratumoral accumulation are ill-defined. We found that interleukin-2 (IL-2) stimulated DC formation through innate and adaptive lymphoid cells in mice and humans, and this increase in DCs improved anti-cancer immunity. Administration of IL-2 to humans within a clinical trial and of IL-2 receptor (IL-2R)-biased IL-2 to mice resulted in pronounced expansion of type-1 DCs, including migratory and cross-presenting subsets, and type-2 DCs, although neither their precursors nor mature DCs had functional IL-2Rs. In mechanistic studies, IL-2 signals stimulated innate lymphoid cells, natural killer cells, and T cells to synthesize the cytokines FLT3L, CSF-2, and TNF. These cytokines redundantly caused DC expansion and activation, which resulted in improved antigen processing and correlated with favorable anti-cancer responses in mice and patients. Thus, IL-2 immunotherapy-mediated stimulation of DCs contributes to anti-cancer immunity by rendering tumors more immunogenic.

ONE SENTENCE SUMMARY

IL-2 immunotherapy expands tumor-infiltrating DCs through a lymphoid pathway, favoring the conversion of poorly immunogenic into immunogenic tumors.

INTRODUCTION

Dendritic cells (DCs) are a subgroup of professional antigen-presenting cells considered indispensable in orchestrating T cell responses to intracellular pathogens and tumors (*1-3*). Human blood DCs have traditionally been subdivided into conventional DCs (cDC) and plasmacytoid DCs (pDC); however, results from single-cell RNA and protein analysis identified additional subpopulations (*4, 5*). In mouse lymphoid organs, DCs are correspondingly divided into cDCs and pDCs. Transcriptionally, cDCs can be further differentiated into type-1 cDCs (cDC1) that are controlled by interferon-regulatory factor 8 (IRF8) and basic leucine zipper transcriptional factor ATF-like 3 (BATF3) and type-2 cDCs (cDC2) that are controlled by IRF4 (*2, 3*). The transcription factor E2-2 regulates pDCs (*3*). Phenotypically, cDC1s are characterized by the presence of CD141 (also known as BDCA-3) and DNGR-1 (also termed CLEC9A) in humans and CD8α, CD103 (also known as integrin αE), DNGR-1, and the chemokine receptor XCR1 in mice. Conversely, cDC2s are marked by CD1c (also referred to as BDCA-1) in humans and CD4 and CD11b in mice (*6*).

DC subsets in non-lymphoid tissues, including the tumor microenvironment (TME), vary considerably in terms of phenotypic and functional properties (*7*). In cancer, rare tumor-infiltrating cDCs attract T cells to the TME, where the cDCs stimulate $CD8^+$ T cells by presenting tumor antigens and producing interleukin-12 (IL-12) (*8-14*). However, the upstream molecular and cellular factors favoring the on-demand generation and expansion of cDCs in anti-tumor responses are ill-defined. Two studies have implicated natural killer (NK) cells in facilitating DC infiltration of tumors, which correlated with prolonged survival in humans (*15, 16*).

NK cells are lymphoid cells, and their survival and homeostasis depends on signals mediated through the common gamma chain cytokine receptor (γc, also termed CD132), encoded by *Il2rg*. Members of the CD132 cytokine family comprise IL-2, IL-4, IL-7, IL-9, IL-15, and IL-21 (*17, 18*). IL-2 signals either through an intermediate-affinity dimeric IL-2 receptor (IL-2R), comprised of IL-2Rβ (CD122) and CD132, or a trimeric IL-2R additionally including IL-2Rα (CD25). The dimeric receptor is found mainly on memory $CD8^+$ T and NK cells, whereas the trimeric receptor is predominantly found on regulatory T (Treg) cells at the steady state and is transiently upregulated on recently activated effector T cells (*17, 19*). In addition to its effects on T cells and NK cells, IL-2 can also stimulate innate lymphoid cells (ILC), particularly type 2 ILCs (ILC2), NKT cells, and activated B cells, as well as certain non-immune cells (*19-21*). However, IL-2 is not known to affect DC homeostasis in vivo.

Thus, it was entirely unexpected to observe a prominent increase in several DC subsets in both mice and humans during our studies on IL-2 immunotherapy. We here describe a pathway driven by IL-2 and mediated by innate and adaptive lymphoid cells. This pathway stimulates DCs and promotes their expansion, processes that contribute to improved anti-tumor immune responses, correlating with prolonged survival in mice and humans.

RESULTS

IL-2 immunotherapy expands cDCs in mice and humans

DCs are characterized by the absence of lineage (Lin) markers, have intermediate (int) or high (hi) CD11c, and can further be subdivided into CD11c^{int} B220^{hi} pDCs, CD11c^{hi} major histocompatibility class II (MHC-II)^{hi} cDCs, CD11b^{low} XCR1^{+} CD8α^{+} DNGR-1 (CLEC9A)$^{+}$ cDC1s, and CD11b^{hi} XCR1^{-} cDC2s (Fig. 1A and fig. S1A). A short course of three injections of recombinant human IL-2 (IL-2; teceleukin) increased total counts of cDCs in spleens of adult wild-type mice (Fig. 1B). This expansion was due to active proliferation of cDCs, as evidenced by increased incorporation of the thymidine analog bromodeoxyuridine (BrdU) into cDCs (Fig. 1C). To assess whether this IL-2 effect was caused by binding of IL-2 to CD25^{hi} or CD122^{hi} cells, we used CD25-biased IL-2/anti-IL-2 (5344) antibody complexes (IL-2/5344) and CD122-biased IL-2/anti-IL-2 (NARA1) antibody complexes (IL-2/NARA1; referred to as IL-2cx exclusively hereafter) (*22-24*). Both CD25-biased and CD122-biased IL-2/anti-IL-2 antibody complexes stimulated qualitatively and quantitatively comparable expansion and proliferation of splenic DCs as unbiased IL-2 (Fig. 1B, C; fig. S1B, C), whereas treatment of *Il2rg*$^{-/-}$*Rag2*$^{-/-}$ mice with IL-2cx did not expand DCs (fig. S1D), thus excluding non-IL-2–mediated stimulation by interactions of anti-IL-2-antibody with Fc receptors on DCs. Moreover, IL-2cx not only mediated expansion of splenic cDCs, but also increased total cDC, cDC1, and cDC2 counts in mouse lymph nodes (fig. S1E).

A detailed analysis of DC subsets showed that administration of IL-2cx expanded counts of all lymphoid-resident cDC subsets, including CD11b^{low} XCR1^{+} cDC1s and CD11b^{hi} XCR1^{-} cDC2s, whereas pDCs remained unchanged compared to untreated mice

(Fig. 1D and fig. S1F). These increased cell counts were accompanied by proliferation of all cDC subsets and pDCs, as evidenced by BrdU positivity (Fig. 1E and fig. S1G).

We also analyzed human $CD11c^+$ MHC-II $(HLA\text{-}DR)^+$ DCs within an investigator-initiated clinical trial (termed Charact-IL-2; NCT 03312335) using recombinant human IL-2 (aldesleukin) immunotherapy (Fig. 1F). We observed an increase in the proliferation of $CD141^+$ cDC1s and $CD1c^+$ cDC2s (Fig. 1G). Different clinical trials testing aldesleukin reported the expected proliferation of $CD4^+$ and $CD8^+$ T cells and NK cells upon aldesleukin immunotherapy (*25, 26*). However, by comparing $Ki67^+$ DCs on day 0 (before) and day 5 (that is 1 day after the last injection) of a 5-day course of daily aldesleukin, we found an increase of proliferating cDC1s and cDC2s (Fig. 1G).

Mature cDCs, identified as $CD11c^{hi}$ MHC-II^{hi} cells that are negative for colony-stimulating factor 1 receptor (CSFR1, also termed CD115), were purified from spleens of control versus IL-2cx–treated mice and submitted to RNA sequencing (RNA-seq). Gene ontology (GO) analysis of the transcriptome of mature cDCs showed overrepresentation of genes associated with cell proliferation and activation of the immune system, including the GO terms cell cycle, cell division, DNA replication, chromosome segregation, nucleosome assembly, protein localization to kinetochore, DNA recombination, chromosome condensation, kinetochore organization, and microtubule depolymerization (Fig. 1H). Other terms, such as response to virus, response to interferon-beta, and response to interferon-alpha, indicated cDCs were exposed to an inflammatory environment (Fig. 1H and fig. S1H). Analyzing the top 75 up- and 75 downregulated genes in more detail, we found the genes in cDCs from the IL-2cx–treated mice were enriched in GO term genes associated with the complement system (*Cfb*, *C3*, *C1qc*, and *C4b*), cytotoxicity (*Gzmb* and

Gzma), and the integrin *Itgae*, which encodes CD103 and is associated with migratory cross-presenting DCs (Fig. 1I). Contrarily, *Cd207*, which encodes Langerin, and certain chemokine receptors and ligands (*Ccl22*, *Cxcl12*, and *Ccr2*) were downregulated. Interestingly, CCL22 was suggested as important in DCs for interaction with $CCR4^+$ regulatory T (Treg) cells, thus implicating CCL22 in the control of excessive T cell responses (*27*).

Taken together, these results established pronounced stimulation of mouse and human cDCs following IL-2 immunotherapy in vivo. This stimulation of DCs resulted in proliferation of both cDC1s and cDC2s.

IL-2 causes proliferation of mature cDCs and differentiation of DC precursors

The observed proliferation and expansion of cDCs could be mediated by proliferation of mature cDCs or differentiation of hematopoietic DC precursors or both. To address this issue, we conducted a cell cycle analysis of mature splenic cDCs using propidium iodide staining. In line with published results stating 5% of lymphoid-resident cDCs are cycling (*28*), we detected 3.2% and 1.9% of splenic cDCs in S and G2/M phase, respectively (Fig. 2A). Proliferating cDCs from mice treated with IL-2cx increased to 10.1% in S and 6% in G2/M phase (Fig. 2A).

To evaluate cDC differentiation from bone marrow precursors, we hierarchically assessed the differentiation steps of DCs, starting from monocyte/DC progenitors (MDP), followed by common DC progenitors (CDP) and the clonogenic progenitors precursor (pre)-cDC1 and pre-cDC2 (Fig. 2B) (*2, 6, 29-33*). IL-2 immunotherapy in mice resulted in a decrease of MDP, CDP, and pre-cDC2 cells in the bone marrow (Fig. 2C), with

simultaneous increase of splenic cDC1 and cDC2 (Fig. 2D). Bone marrow pre-cDC1 cells did not change, possibly due to compensatory proliferation (Fig. 2C). Because CD135 is used to identify DC precursors, the observed decrease in bone marrow counts could be partly impacted by downregulation of CD135 upon engagement with its ligand FLT3L.

Investigating the possibility that IL-2 treatment impacts survival of cDCs, we measured intracellular caspase 3, which induces apoptosis downstream of the intrinsic pathway regulated by the B cell leukemia 2 (BCL-2) protein family and the extrinsic pathway mediated by death receptors activated at the cell surface (*34*). However, we did not observe any significant difference in caspase 3-positive splenic cDCs between untreated and IL-2cx–treated mice (Fig. 2E; $P = 0.6794$). Staining for live cells versus dead cells with Annexin-V and 7-AAD confirmed these results (fig. S2A). Additionally, in the intrinsic apoptosis pathway, neither the amount of BCL-2, which is the inhibitor of the pro-apoptotic BCL-2-associated X (BAX) protein (*35*), nor the amount of BAX was different between cDCs from untreated and IL-2cx–treated mice (fig. S2, B and C). These results suggested no survival benefit after IL-2 treatment, yet they were measured indirectly by apoptosis-regulating proteins. Direct measurement of survival by adoptive transfer of cDCs from untreated and IL-2cx–treated mice into untreated recipients revealed a small, but significant, survival advantage of the IL-2cx–treated cDCs (Fig. 2F, $P = 0.0015$). Due to the increased differentiation of DC progenitors this effect could be attributed to the inclusion of 'younger' cDC subsets in the transferred cDCs from IL-2cx–treated mice. To exclude this possibility, we reversed the experimental setup and transferred cDCs from untreated mice to either untreated or IL-2cx–pretreated mice, observing a small, but insignificant increase in the IL-2cx–pretreated mice (Fig. 2G; $P = 0.3148$).

Together, these results suggested that IL-2 treatment facilitates proliferation of mature cDCs and accelerated differentiation of DC progenitors to mature DCs. To a lesser extent, IL-2 treatment might enhance DC survival.

Mature DCs and their precursors lack functional IL-2Rs

Given the profound stimulatory effects of IL-2 on cDCs, we investigated IL-2R abundance on cDCs and their precursors at the mRNA and protein levels. Quantitative polymerase chain reaction (qPCR) of *Il2r* transcripts from untreated and IL-2cx–treated cDCs, $CD4^+$ $Foxp3^-$ conventional T (Tcon) and $CD4^+$ $Foxp3^+$ Treg cells revealed that cDCs contained *Il2rg* mRNA, but they lacked *Il2ra* or *Il2rb* mRNA (Fig. 3A). In comparison, Tcon and Treg cells expressed mRNA for all three IL-2R subunits (Fig. 3A). We also confirmed these results at the protein level by surface staining for IL-2R subunits on mature mouse cDCs and Treg cells in untreated and IL-2cx–treated mice (Fig. 3B). As previously published (*36, 37*), cDCs upregulated CD25, but not CD122, upon stimulation with two different Toll-like receptor ligands (fig. S3A). We investigated IL-2R abundance on DC precursors. MDP and CDP lacked detectable amounts of CD132; pre-cDC1 had a slightly detectable amount of CD132 and pre-cDC2 had clearly detectable CD132 (Fig. 3C). MDP, CDP, pre-cDC1, and pre-cDC2 all lacked detectable surface CD122 and CD25, even following IL-2cx treatment (Fig. 3C and fig. S3B).

To directly assess whether mature cDCs had functional IL-2Rs, we analyzed downstream intracellular signaling by signal transducer and activator of transcription 5 (STAT5), which becomes phosphorylated (pSTAT5) upon activation of a functional IL-2R by IL-2. As a positive control for STAT5 signaling, we also tested the cDCs response to

colony-stimulating factor 2 (CSF2; also termed granulocyte-macrophage colony-stimulating factor), which also activates STAT5. Confirming the lack of functional IL-2Rs, even the highest concentrations of IL-2 tested failed to induce pSTAT5 in cDCs, whereas Treg cells readily responded to the same range of IL-2 concentrations in a dose-dependent manner (Fig. 3D). Conversely, pSTAT5 increased in cDCs incubated with mouse CSF2, whereas Treg cells remained unaffected by this stimulation (Fig. 3D). The same results applied to cDCs from IL-2cx–treated mice (fig. S3C). Furthermore, Lin^- $CD135^+$ DC precursors, including MDPs, CDPs, pre-cDC1s, and pre-cDC2s, from untreated and IL-2cx–treated mice did not show increased pSTAT5 upon stimulation with a high dose (1,000 IU) of IL-2, whereas incubation with mouse CSF2 increased pSTAT5 (fig. S3D). Thus, DC precursors do not have functional IL-2Rs.

Similar to their mouse counterparts, human cDCs were positive for CD132 but lacked detectable CD25 and CD122 at the cell surface, unlike $CD4^+$ T cells that served as controls (Fig. 3E). Accordingly, stimulation of human cDCs with a high IL-2 concentration did not increase pSTAT5, whereas the same treatment induced pSTAT5 in human $CD4^+$ T cells, and human CSF2 increased pSTAT5 in human cDCs (Fig. 3F).

Supporting these findings, IL-2cx treatment of bone marrow chimeric mice carrying a 1:1-mix of CD45.1-congenic wild-type and CD45.2-congenic *Il2rg*$^{-/-}$ DCs resulted in equal expansion of both wild-type and *Il2rg*$^{-/-}$ cDCs (Fig. 3G). Collectively, these data support a model whereby IL-2 immunotherapy indirectly activates cDCs and their precursors through the induction of intermediary factors.

IL-2 immunotherapy causes production of several DC mitogens

Searching for candidates that stimulate cDCs and their precursors, we decided to assess FMS-like tyrosine kinase 3 ligand (FLT3L) and CSF2, because these cytokines contribute to the development and survival of DCs during steady state and inflammation, respectively (*38*). Untreated *Flt3l*$^{-/-}$ mice had reduced cDC counts compared to wild-type mice, amounting to ~1 × 10^6 per spleen in wild-type (Fig. 1B) versus ~2.5 × 10^4 per spleen in *Flt3l*$^{-/-}$ (Fig. 4A), thus confirming the importance of FLT3L for cDC homeostasis. However, similar to wild-type mice (Fig. 1B), IL-2 treatment caused a 4-fold expansion of cDCs in *Flt3l*$^{-/-}$ animals (Fig. 4A). Likewise, use of IL-2cx in *Csf2*$^{-/-}$ mice, which contained reduced steady-state numbers of cDCs compared to those in wild-type, resulted in an increase of splenic cDC counts (Fig. 4B). We predicted that FLT3L and CSF2 compensated for the absence of each other, but surprisingly, *Flt3l*$^{-/-}$ *Csf2*$^{-/-}$ double-knockout mice also showed expansion and proliferation of cDCs and corresponding subsets upon IL-2 treatment (Fig. 4, C and D, and fig. S4A).

In previous experiments, we observed that IL-2cx treatment increased tumor necrosis factor (TNF) in a T cell-dependent manner (*39*). We thus hypothesized that TNF stimulates cDC expansion in *Flt3l*$^{-/-}$ *Csf2*$^{-/-}$ mice. Indeed, blocking TNF with the soluble TNF receptor 2-Fc-IgG1 fusion protein etanercept reduced cDC expansion to close to background amounts in IL-2cx–treated animals (Fig. 4E). Etanercept treatment of wild-type mice also reduced expansion and proliferation of cDCs, suggesting a FLT3L– and CSF2–independent effect of TNF on DC homeostasis (Fig. 4F and fig. S4B). Moreover, IL-2cx treatment of bone marrow chimeric mice containing a 1:1-mix of wild-type and *Tnfrsf1a/b*$^{-/-}$ bone marrow reduced expansion of *Tnfrsf1a/b*$^{-/-}$ cDCs, thus indicating a direct effect of TNF on cDCs (Fig. 4G).

Measurement of serum cytokines in mice showed marked increase in FLT3L and TNF upon IL-2 immunotherapy, whereas CSF2 was not detectable (Fig. 4H). The latter might be due to local action of CSF2 rather than systemic secretion (*38*). We found similar results for these cytokines in human serum before and after aldesleukin treatment (Fig. 4I). In summary, these results indicated that IL-2 mediates cDC expansion through secretion of the cytokines FLT3L, CSF2 and TNF, all of which directly stimulate cDCs (referred to hereafter as DC-active cytokines).

IL-2–stimulated innate and adaptive lymphoid cells produce DC-active cytokines

Our results indicated that cDCs were expanded by cytokines secreted by IL-2–responsive cells. Because both hematopoietic cells and non-hematopoietic cells have IL-2Rs (*23*), we investigated whether cDC-stimulating cells are of hematopoietic origin. To this end, we generated bone marrow chimeric mice in which wild-type or *Il2rg*$^{-/-}$ recipients were lethally irradiated (950 RAD) and reconstituted with wild-type or *Il2rg*$^{-/-}$ bone marrow (Fig. 5A, left). Only mice reconstituted with wild-type bone marrow, but those not with *Il2rg*$^{-/-}$ bone marrow, showed expansion of splenic cDCs after IL-2 immunotherapy, indicating that IL-2–responsive cells are of hematopoietic origin (Fig. 5A).

To evaluate potential target cells, we searched the ImmGen database (*40*) to identify mouse immune cells with functional IL-2Rs, comprising at least those with both CD122 and CD132. By examining *Il2ra*, *Ilr2b*, and *Il2rg* expression, our search revealed that, in addition to T, NK, and NKT cells, ILCs had detectable amounts of each of these transcripts (fig. S5A). As previously published (*22-24, 39, 41, 42*), we confirmed in vivo expansion and proliferation of CD4^{+} T, CD8^{+} T, and NK cells upon IL-2cx treatment (fig. S5, B to

D). Furthermore, all ILC subsets, including type-1 ILCs (ILC1), type-2 (ILC2), and type-3 (ILC3), showed proliferation and expansion upon IL-2 immunotherapy (Fig. 5B and fig. S5E).

To assess the contribution of each IL-2–responsive cell subset to cDC homeostasis and IL-2–mediated cDC expansion, we used different knockout and antibody-depletion strategies. Although *Tcrbd*$^{-/-}$ mice, lacking both αβ and γδ T cells, showed reduced counts of splenic cDCs compared to wild-type, amounting to ~1 × 10^6 per spleen in wild-type (Fig. 1B) versus ~3 × 10^5 per spleen in *Tcrbd*$^{-/-}$ (Fig. 5C), IL-2cx treatment stimulated expansion of cDCs in the *Tcrbd*$^{-/-}$ animals (Fig. 5C). We used *Rag1*$^{-/-}$ mice, lacking T and B cells, and depleted the mice of NK cells, ILCs, or both by injection of anti-NK1.1 or anti-Thy1.2 antibodies or both antibodies. Both cell types contributed to IL-2–mediated cDC expansion (Fig. 5D). The incomplete inhibition of cDC expansion in *Rag1*$^{-/-}$ mice depleted of NK cells and ILCs is likely due to tissue residency of ILCs, which are incompletely amenable to antibody-mediated depletion (*43*).

To further study the contribution of ILCs to IL-2–induced cDC proliferation, we reconstituted sublethally irradiated (450 RAD) *Il2rg*$^{-/-}$ and *Il2rg*$^{-/-}$ *Rag2*$^{-/-}$ mice with ILC2 precursor (ILC2p) cells (Fig. 5E and fig. S5F) (*43-45*). Two months later, ILC2p cells had developed to all ILC subsets but not into B, T, and NK cells (Fig. 5F, upper panel). Although sorted ILC2p cells were used for the reconstitution of *Il2rg*$^{-/-}$ *Rag2*$^{-/-}$ mice, we detected not only ILC2s, but also RORγt$^+$ ILC3s and RORγt$^-$ GATA3$^-$ ILC1s (Fig. 5F, upper panel). Control mice reconstituted with common lymphoid progenitor (CLP) cells harbored all ILC subsets, as well as B, T, and NK cells (Fig. 5F, lower panel). Subsequent

treatment with IL-2cx induced the expansion of splenic cDCs in ILC2p-reconstituted mice (Fig. 5G).

To investigate whether lymphoid cells produced cDC-active cytokines, we measured intracellular RNA transcripts of FLT3L, CSF2 and TNF with flow cytometry, which showed that T, NK cells, and ILCs produced *Flt3l* at steady state (Fig. 5H). IL-2 treatment of mice further stimulated production in $CD4^+$ Treg, $CD8^+$ T, and NK cells, but not in $CD4^+$ Tcon cells and ILCs (Fig. 5H). Under steady-state conditions, low amounts of *Csf2* transcripts were detected, and IL-2cx treatment of mice induced expression in NK cells, ILC1, and ILC2, but not in T cells and ILC3 (Fig 5H). IL-2 treatment of mice increased intracellular *Tnf* in all subsets (Fig. 5H).

Intracellular assessment of CSF2 and TNF upon in vitro stimulation confirmed expansion of $CSF2^+$ and TNF^+ cells in all investigated lymphocyte subsets and ILCs, except for TNF^+ $CD4^+$ Tcon cells, which did not expand (Fig. 5, I and J). Together, these results demonstrated that IL-2 stimulates innate and adaptive lymphoid cells to produce DC-active cytokines, which then stimulate the expansion of cDCs.

IL-2 immunotherapy-activated cDCs facilitate anti-tumor responses in mouse and human

We investigated the effects of IL-2 treatment on the function of cDCs. Treatment of mice with IL-2cx induced upregulation of CD40, CD80, CD86, and MHC class I (MHC-I), but not MHC-II, on cDCs (Fig. 6A). These changes are indicative of mature cDCs with increased potential of cross-presentation and co-stimulation for T cell activation (*10, 46,*

47). RNA-seq data confirmed that cDCs from IL-2–treated animals showed upregulation of genes associated with antigen processing and presentation (fig. S6A).

To measure antigen uptake and processing, we used DQ-ovalbumin in which fluorescence is an indirect measure of lysosomal degradation of ovalbumin in cDCs. Compared with cDCs from untreated mice, cDCs from IL-2cx–treated mice showed greater antigen uptake and processing after 24, 48, and 72 hours of in vitro culture (Fig. 6B).

Based on these data, we hypothesized that cDCs from IL-2–treated mice have greater capacity to activate T cells than those from untreated mice. We isolated cDCs from untreated or IL-2cx–treated mice, incubated these cells with a 24-amino-acid-ovalbumin peptide (DEVSGLEQLESIINFEKLAAAAAK) with improved cross-presentation properties (*48*), and adoptively transferred these cDCs into naïve mice by footpad injection. After 24 hours, carboxyfluorescein succinimidyl ester (CFSE)-labelled antigen-specific OT-1 $CD8^+$ T cells were adoptively transferred into the mice and the proliferation of these T cells was assessed 2 – 3 days later (Fig. 6C). The results confirmed our hypothesis: cDCs from IL-2cx–treated animals induced significantly more expansion of OT-1 $CD8^+$ T cells (Fig. 6C; $P = 0.0206$).

To investigate whether IL-2 immunotherapy expanded tumor-infiltrating cDCs, we quantified cDCs in B16-F10 melanoma-bearing mice receiving IL-2cx (fig. S6B). Tumor-infiltrating $CD103^+$ cDC1s and cDC2s were increased on day 11 after tumor implantation, and tumor growth was delayed in IL-2cx–treated compared to growth in untreated mice (Fig. 6D). On the contrary, anti-PD-1 antibody treatment neither increased tumor-infiltrating $CD103^+$ cDC1s or cDC2s, nor delayed tumor growth compared to untreated animals (Fig. 6D and fig. S6C). The failure of anti-PD-1 monotherapy to reduce growth of

B16-F10 melanoma is consistent with observations of other groups (*49, 50*). Further analyzing these data, we observed a negative linear correlation between tumor-infiltrating cDC1 and tumor volume (Fig. 6E). We did not observe a significant correlation for tumor-infiltrating cDC2 (Fig. 6E; $P = 0.0872$). We observed increased numbers of tumor-infiltrating cDC1 and cDC2 in the inducible melanoma model *Braf*^{CA} *Pten*^{loxP} *Tyr::CreERT2* (Fig. 6F).

To clarify the role of cDCs in orchestrating IL-2–mediated anti-tumor responses, we evaluated B16-F10 melanoma growth in two different DC-depletion models: The *Cd11c*-DTR model, which depletes all CD11c^{+} cells upon administration of diphtheria toxin (DT), and the *Zbtb46*-DTR model, which specifically depletes cDCs (*3*). In bone marrow chimeras generated using these transgenic mice, IL-2cx–mediated tumor control was lost when DCs were continuously depleted beginning 1 day before tumor implantation (Fig. 6, G and H, and fig. S6, D and E). DC-depleted mice not receiving immunotherapy did not show accelerated tumor growth compared with mice that were not DC depleted, likely due to the aggressive growth of B16-F10 melanoma. Similar to the other B16-F10 results (Fig. 6D), anti-PD-1 treatment did not delay tumor growth.

Analyzing TCGA data of human skin cutaneous melanoma revealed prolonged survival of patients with tumors with a high IL-2 signature, consisting of *IL2* and 10 IL-2–induced genes (*51*) (50% threshold; Fig. 6I). We observed a similar trend for patients with *BATF3*^{high} tumors (Fig. 6I). Notably, the hazard ratio for tumors with high expression of the IL-2 signature was even lower than that for *BATF3*^{high} tumors (hazard ratio 0.57 and 0.68, respectively), suggesting the IL-2 signature has a better predictive value. Further data mining uncovered a positive relationship between the IL-2 signature and *BATF3* (Fig. 6J).

Other correlations were found between *BATF3* and *CD4*, *CD8B,* and an NK cell signature (Fig. 6K). *BATF3* also correlated with the *CSF2-FLT3L-TNF* cytokine signature and the individual cytokines *CSF2*, *FLT3L*, and *TNF* (Fig. 6L). More detailed analysis revealed a positive correlation between *IL2* and *BATF3* as well as between each *IL2R* subunit transcript and *BATF3* (fig. S6F).

Altogether, these data showed that IL-2 immunotherapy promotes activation and expansion of tumor-infiltrating cDCs, which enhances antigen presentation and $CD8^+$ T cell activation. These effects correlated with improved anti-tumor responses in mice and humans.

DISCUSSION

Previous seminal studies established a crucial role of intratumoral $CD103^+$ cDCs in stimulating $CD8^+$ T cells for efficient anti-tumor responses (*8-11*). These cells depend on FLT3L, CSF2, BATF3, and IRF8. However, these cells are extremely rare in the TME. Our work identified an IL-2–lymphoid cell–cDC pathway that robustly expands and stimulates this $BATF3^+$ $IRF8^+$ $CD103^+$ cDC1 subset. This pathway depended on production of FLT3L, CSF2, and TNF by several ILC subsets, NK cells, and T cells. These DC-active cytokines induced differentiation of DC precursors, as well expansion and activation of mature cDCs. Thus, our findings extend work showing that NK cells attract DCs into the TME by secreting XCL1 and CCL5 (*15*) and serve as the main producers of FLT3L in mouse melanoma (*16*). Moreover, we showed that the IL-2–lymphoid cell–cDC pathway stimulates and expands cDC2s, which have been implicated in priming anti-tumor $CD4^+$ T cell responses (*46*). Although FLT3L and CSF2 play critical roles in cDC expansion (*28, 38*), TNF induces cDC maturation that is critical for efficient anti-viral responses (*52*). Our findings suggested a role for TNF in cDC differentiation in vivo, supporting previous studies showing such an effect in vitro where TNF skews differentiation of precursors from monocytes to DCs by inhibiting the IL-6/CSF1 pathway (*53*).

Some previous studies suggested that DCs have functional IL-2R and that IL-2 has a direct effect on DC development in vitro (*54, 55*); other studies provided somewhat contradictory data based on the absence of CD122 on DCs (*56-58*). Mouse (*59*) and human (*60*) DCs can have detectable CD25, especially upon stimulation with TLR ligands (*36, 37*) or following culture with CSF2 (*56*). Functionally, upregulation of CD25 on activated

DCs could facilitate trans-presentation of IL-2 to T cells early during T cell activation (*61, 62*). Concerning CD122, most studies suggest that directly isolated or CSF2-cultured mouse and human DCs do not have detectable CD122 (*56-58*). Nevertheless, two carefully conducted in vitro studies suggested an inhibitory role of IL-2 on FLT3L-mediated DC differentiation from mouse bone marrow (*54, 55*). The discrepancy between the observed inhibitory effect of IL-2 and our study might be explained by the different conditions, cytokines, and other growth factors in vitro versus in vivo. Here, neither directly isolated DCs nor DC precursors had CD122, even after in vivo IL-2 or TLR ligand treatment. Furthermore, we could not detect activation of the IL-2 signaling pathway after incubation of DCs and DC precursors with high concentrations of IL-2, which to our knowledge has not been shown in previous studies claiming functional IL-2Rs on DCs. Thus, DCs and DC precursors do not have functional IL-2Rs. Finally, *Il2rg*$^{-/-}$ cDCs expanded equally to *Il2rg*$^{+/+}$ cDCs in bone marrow chimeric mice upon IL-2 treatment, strongly supporting our model of indirect DC expansion through secondary secretion of DC-active cytokines upon IL-2 treatment in vivo.

Our work thus uncovers an aspect of IL-2–mediated anti-tumor responses beyond the direct effects on IL-2–responsive effector cells. One could speculate that IL-2 treatment might turn poorly immune infiltrated, that is 'cold', tumors into highly infiltrated, 'hot' tumors, which are responsive to immune checkpoint inhibitors. In line with this suggestion, IL-2 immunotherapy in melanoma-bearing mice increases intratumoral TNF and CCL5 production and PD-1 ligand (PD-L1) abundance on cancer cells, thus rendering the tumor hot (*39*). Moreover in patients, treatment with the PEGylated IL-2 molecule bempegaldesleukin (also known as NKTR-214) increased PD-L1 on previously PD-L1–

negative urothelial cancer biopsies after 3 weeks of treatment, indicating the conversion of a cold to a hot TME (*63*).

Furthermore, our data could explain why IL-2 immunotherapy has in some patients resulted in remarkably long-term anti-tumor responses lasting 20 years and more (*64*). This finding could indicate the priming and programming of long-lived memory $CD8^+$ and $CD4^+$ T cells during IL-2 immunotherapy by direct IL-2 signals (*65*) and restimulation of $CD8^+$ and $CD4^+$ T cells by IL-2–mediated expansion of intratumoral cDC1s and cDC2s. Based on this suggestion, we hypothesize that the herein-described adaptive cDC-poiesis could affect the generation and development of long-lived memory $CD8^+$ T cells. These suggestions might also apply to bacterial and viral infections. Thus, early cDCs presenting high loads of antigens could prime T cells to preferentially adopt a short-lived effector fate, whereas a second wave of cDCs due to the IL-2–lymphoid cell–cDC pathway could result in cDCs carrying lower concentrations of antigenic peptides, thereby inducing memory T cells.

Future studies should address the following limitations of our study. Our patient tumor results are derived from the TCGA database and reflect correlations between different gene signatures. It would be interesting to extend our investigations to melanoma patient samples from tumors and secondary lymphoid tissues, ideally in a paired manner before and after high-dose aldesleukin treatment. However, these samples are very difficult to obtain as aldesleukin has rarely been used for cancer immunotherapy to date. Furthermore, our investigations have focused on mouse and human melanoma. Assessment of other cancer types following IL-2 immunotherapy could reveal a similar pathway that results in DC expansion. Another topic concerns depletion of ILCs. Using monoclonal

antibodies targeting NK cells and ILCs only partially abrogated IL-2cx–mediated DC expansion. This could be due to incomplete depletion of tissue-resident ILCs, which should be assessed in future studies using transgenic mouse models allowing specific and complete depletion of selective ILC subsets.

In summary, our work further sheds light on an IL-2 immunotherapy-mediated IL-2–lymphoid cell–cDC pathway (fig. S7). Our findings support the investigation of potential combinatorial approaches in which IL-2 treatment could render poorly immunogenic cancers amenable to treatment with immune checkpoint inhibitors.

MATERIALS AND METHODS

Study design

The aim of this study was to assess the mechanism of IL-2–mediated DC expansion in mice and humans. To this end, we used different mouse models, blood samples collected from IL-2–treated patients, and publicly available datasets. Sample size was chosen empirically based on results of previous studies. Reporting of mouse studies followed the Animal Research: Reporting of In Vivo Experiments (ARRIVE) guidelines. In general, experiments aimed to include in total 10 mice per group and were repeated three times with precise numbers for each individual experiment provided in the figure legends. Mice were randomly assigned to different treatment groups and stratified according to gender and age. Investigators were not blinded. No data outliers were excluded. Primary data are reported in data file S1.

Clinical trial and human samples

Human samples were collected within the clinical trial "Open-label, Monocentric, Phase II, Investigator-initiated Clinical Trial on Unbiased Characterization of Immunological Parameters in Interleukin-2-treated Systemic Lupus Erythematosus" (Charact-IL-2, ClinicalTrials identifier: NCT03312335) and the "Fundamental research project for phenotypical and functional characterization of different leukocyte subsets in healthy and diseased individuals" (PFCL-1, BASEC no. 2016-01440). Both projects have been reviewed and approved by the competent Swiss authorities and have been carried out in accordance with principles enunciated in the current version of the Declaration of Helsinki, the guidelines of Good Clinical Practice, and Swiss legal requirements. Prior to enrollment

into the clinical trial or sample collection, written informed consent was obtained. Human blood was collected into EDTA Vacutainer tubes (BD Biosciences) followed by Ficoll-Paque PLUS (GE Healthcare) gradient centrifugation for peripheral blood mononuclear cell (PBMC) isolation. Isolated PBMCs were frozen in fetal calf serum (FCS, Gibco) containing 10% dimethyl sulfoxide (Sigma) and stored for less than 1 year in liquid nitrogen prior to analysis. Serum was isolated from blood collected with Clot Activator Vacutainer tubes (BD Biosciences) and stored for less than 18 months at –80°C prior to analysis.

For evaluation of IL-2–mediated expansion of cDCs and lymphocytes, blood from patients with systemic lupus erythematosus (SLE) was collected prior and after a 5-day course of daily 1.5 million international units (MIU) of aldesleukin (Proleukin®, Novartis Pharma), according to the study protocol.

Mice

C57Bl/6J mice were purchased from Charles River Laboratories. *Tcrbd*$^{-/-}$ (JAX stock no. 002122), *Rag1*$^{-/-}$ (JAX stock no. 002216), *Csf2*$^{-/-}$, *Flt3l*$^{-/-}$, CD45.1^{+} (JAX stock no. 002014), *Il2ra*$^{-/-}$ (JAX stock no. 002462), *Il2rb*$^{-/-}$ (JAX stock no. 002816), *Il2rg*$^{-/-}$ (JAX stock no. 003174), *Rag2*$^{-/-}$ *Il2rg*$^{-/-}$ (Taconic stock no. 4111), OT-1 (JAX stock no. 003831), *Cd11c*-DTR (JAX stock no. 004509), *Zbtb46*-DTR (JAX stock no. 019506), *Tnfrsf1a/b*$^{-/-}$ (JAX stock no. 003243), *Foxp3*-GFP-DTR (JAX stock no. 016958), and *Braf*^{CA} *Pten*^{loxP} *Tyr::CreERT2* (JAX stock no. 013590) were obtained from the Jackson Laboratory (JAX) or from the Swiss Immunology Mouse Repository. *Csf2*$^{-/-}$ (JAX stock no. 026812) and *Flt3l*$^{-/-}$ (MMRRRC stock no. 37395-JAX) mice were generously provided by M. Manz

(University Hospital Zurich) and A. Rolink (University of Basel), respectively, and crossed to generate *Csf2*$^{-/-}$ *Flt3l*$^{-/-}$ mice. Female and male mice were used for experiments at 2 – 5 months of age. The experiments were conducted in a randomized fashion by unblinded investigators. Mice were held in a specific pathogen free (SPF) facility at the University Hospital Zurich according to institutional guidelines. Animal experiments received prior approval by the veterinary office of the Canton of Zurich (License numbers 142/2017 and 246/2016) and were conducted in accordance with Swiss Federal and Cantonal Law.

In vivo treatments

Recombinant human IL-2 (teceleukin, Roche) was obtained from the National Cancer Institute of the National Institutes of Health. IL-2/NARA1 (IL-2cx) and IL-2/5344 antibody complexes were prepared by mixing 15,000 IU IL-2 and 15 µg anti-IL-2 monoclonal antibodies (mAbs) per injection, as previously described (*22-24*). IL-2cx, IL-2/5344 antibody complexes, or 200,000 IU IL-2 were injected daily for three consecutive days unless stated otherwise. Where mentioned, depletion of specific immune cells was performed using 250 µg anti-NK1.1 mAb (clone PK136, Leinco Technologies) and 500 µg anti-Thy1.2 mAb (clone 30H12, BioXcell). Depleting mAbs were administered intraperitoneally daily throughout the experiment starting one day before treatment initiation with IL-2 complexes. For in vivo activation of DCs, 100 µg polyinosinic–polycytidylic acid (Poly I:C; Sigma-Aldrich) and 100 µg Pam3Csk4 (InvivoGen) was injected daily for three consecutive days.

To determine immune cell proliferation, bromodeoxyuridine (BrdU; B5002, Sigma-Aldrich) was given to mice either by daily i.p. injection (1 mg/injection) or in

drinking water (0.8 mg/ml), as established (*66*). BrdU-incorporated cells were labeled using the FITC BrdU Flow Kit (BD Biosciences) according to manufacturer's instructions.

Where indicated, 500µg etanercept (Enbrel®, Pfizer) was injected concomitantly with IL-2cx for three consecutive days.

Flow cytometry

Single cell suspensions of lymph nodes, spleens, and bone marrow were prepared according to standard protocols. For all experiments evaluating DCs, organs were digested in PBS containing 1 mg/ml collagenase D (Roche) for 15 min in the incubator at 37°C. Tumors were cut into small pieces and incubated in 10 ml dissociation buffer (RPMI, 5% FCS, 10 µg/ml DNAse I (Sigma-Aldrich) and 200 U/ml collagenase type I (Thermo Fisher Scientific) for 60 min at 37°C, shaking with 25 rpm. Cell suspensions were then passed through a 70-µm cell strainer. In experiments with intradermally implanted tumors, after one wash a Percoll (40% and 70%; GE Healthcare) gradient centrifugation was performed. All cell suspensions were stained for flow cytometry analysis using flow cytometry buffer (PBS with 2% FCS, 2 mM EDTA) and fluorochrome-conjugated antibodies for at least 20 min at 4°C. A list of used antibodies is provided in table S1. Intracellular staining with Ki67, FOXP3, GATA3, RORγt, TBET, BAX, BCL-2, CSF2, and TNF was performed following manufacturer's instructions using the eBioscience™ Foxp3 / Transcription Factor Staining Buffer Set (ThermoFisher). Caspase-3 was measured with the Active Caspase-3 Apoptosis Kit (BD Biosciences) according to manufacturer's instructions. Annexin V and 7-AAD live and dead cell staining was conducted according to the instructions of the Annexin V Apoptosis Detection Kit with 7-AAD (BioLegend).

For STAT5 phosphorylation analysis, freshly isolated mouse splenocytes or human PBMCs were incubated for 25 min at 37°C as indicated with either mouse CSF2 (Peprotech), human CSF2 (Peprotech), or IL-2 (teceleukin, Roche). Cells were directly fixed with paraformaldehyde (Sigma-Aldrich, final concentration 1.5%) followed by permeabilization with methanol (Cantonal Pharmacy Zurich) and staining with fluorochrome-conjugated antibodies in flow cytometry buffer.

Cell cycle analysis was conducted with FxCycle PI/RNase Staining Solution (Thermo Fisher Scientific) after ethanol fixation (Cantonal Pharmacy Zurich, final concentration 70%) according to manufacturer's instruction.

Intracellular RNA was measured with PrimeFlow RNA assay (Thermo Fisher Scientific) with target probes against *Actb* (Ref 60384), *Flt3l* (Ref 64644), *Csf2* (Ref 64983), and *Tnf* (Ref 60209) according to manufacturer's instructions.

Samples were acquired with a BD FACS Canto II, BD LSR II, or BD FACSymphony flow cytometer (BD Biosciences) and analyzed using FlowJo software (BD Biosciences). Where indicated, fluorescence-activated cell sorting (FACS) was performed using a BD FACS Aria III 5L (BD Biosciences).

Generation of bone marrow chimeras

Bone marrow chimeric mice were generated by adoptive transfer of $1 – 2 \times 10^6$ lineage (Lin)-depleted bone marrow cells from donor mice into lethally (950 RAD) irradiated host mice. Lineage depletion was done by magnetic negative selection (MoJoSort Streptavidin Nanobeads, BioLegend) with biotinylated antibodies targeting CD3, CD19, NK1.1, and Ter119 (all from BioLegend). For ILC reconstitution experiments, ILCp ($CD127^+$ $\alpha4\beta7^+$

CD25^{+} CD135^{-} CD117^{-}) and, where indicated, CLPs (CD127^{+} α4β7^{-} CD135^{+}) were FACS-sorted from Lin^{-} (CD3, CD4, CD5, CD8, CD11b, CD11c, CD19, CD335, B220, Gr-1, Ter119, NK1.1, F4/80) bone marrow, followed by adoptive transfer into sublethally (450 RAD) irradiated *Il2rg*$^{-/-}$ or *Il2rg*$^{-/-}$ *Rag2*$^{-/-}$ mice. All mice were rested for at least 6 – 8 weeks prior to treatment with IL-2cx.

Cell cultures

For DQ-ovalbumin assays, splenocytes were isolated as described above followed by incubation in DQ-ovalbumin (Life Technologies) at a concentration of 50 µg/ml in full RPMI medium [RPMI (Gibco) containing 10% FCS (Gibco), 4 mM L-glutamine (Thermo Fisher Scientific), and Penicillin-Streptomycin (Thermo Fisher Scientific)] for the time indicated.

For intracellular TNF or CSF2 measurements in lymphocytes, splenocytes of wild-type mice were stimulated for 4 or 8 hours in full RPMI medium containing either 50 ng/ml phorbol 12-myristate 13-acetate (PMA, Sigma-Aldrich), 0.5 µg/ml ionomycin (Sigma-Aldrich), and 10 µg/ml brefeldin A (BFA, Sigma-Aldrich) for TNF evaluation; or 100 ng/ml PMA, 1 µg/ml ionomycin, and 2 µM monensin (BioLegend) for CSF2 evaluation. For intracellular TNF and CSF2 measurements in ILCs, splenocytes of *Tcrbd*$^{-/-}$ mice were stimulated for 6 hours in full RPMI medium containing 100 ng/ml PMA, 1 µg/ml ionomycin (Sigma-Aldrich), and 10 µg/ml brefeldin A (BFA, Sigma-Aldrich).

Adoptive DC transfer by intrasplenic injection

For studies assessing the persistence of mature DCs, cell trace violet-labeled (labeling for 7.5 min at 37°C; Thermo Fisher Scientific), magnetically purified $CD11c^+$ (MoJoSort Mouse CD11c Nanobeads, BioLegend) splenocytes isolated from untreated or IL-2cx–pretreated $CD45.1^+$ or $CD45.2^+$ mice were adoptively transferred by subcapsular injection into the spleen of either untreated (Fig. 2F) or IL-2cx–pretreated recipients (Fig. 2G). IL-2cx–treated donors received IL-2cx on three consecutive days before isolation of splenocytes, whereas IL-2cx–treated recipients received IL-2cx on three consecutive days with the last injection coinciding with the day of adoptive DC transfer.

OT-1 proliferation

CD45.1 mice were treated with IL-2cx for 3 consecutive days or left untreated followed by isolation of splenocytes and magnetic purification of $CD11c^+$ cells with (MojoSort Mouse CD11c Nanobeads, BioLegend). Isolated cells were incubated in RPMI (Gibco) containing 10% FCS (Gibco), 4 mM L-glutamine (Thermo Fisher Scientific), Penicillin-Streptomycin (Thermo Fisher Scientific), and 50 µg/ml ovalbumin peptide (DEVSGLEQLESIINFEKLAAAAAK, obtained from the peptide synthesis facility of Leiden University Medical Center) for 2 hours before injection into the foot pad of CD45.2 recipient mice (*48*). 2-3 x 10^6 purified and carboxyfluorescein succinimidyl ester (CFSE; Thermo Fisher Scientific)-labeled OT-1 T cells were adoptively transferred to recipients 24 hours later and proliferation measured 2 – 3 days after adoptive transfer.

Tumor experiments

The mouse B16-F10 (CRL-6475, ATCC) cell line was cultured in Advanced DMEM (Gibco) containing 10% FCS (Gibco), 4 mM L-glutamine (Thermo Fisher Scientific), and Penicillin-Streptomycin (Thermo Fisher Scientific). Recipient mice were intradermally engrafted with 1×10^6 B16-F10 cells. Treatment was started when tumor nodules were visible and palpable on day 4 after tumor inoculation by using IL-2cx or 100 µg anti-PD-1 (clone RMP1-14, Leinco Technologies) injected every other day (fig. S6B, upper panel) (*24*). Mice were euthanized on day 11 for isolation of tumor-infiltrating lymphocytes. For evaluating tumor growth under DC-deficient conditions, lethally irradiated C57Bl/6J host mice were reconstituted with Lin-depleted *Cd11c*-DTR or *Zbtb46*-DTR bone marrow, as described above, followed by treatment with 0.5 µg DT (Sigma-Aldrich) 3× weekly starting one day prior to tumor inoculation. IL-2cx and anti-PD-1 treatment was continuously administered 3× weekly starting day 4 after tumor inoculation (fig. S6B, lower panel). Tumor volume was calculated according to the following formula: $V = 2/3 \times \pi \times ((a + b)/4)^3$, a (mm) was the length and b (mm) was the width of the tumor.

For inducible tumors, *Braf*^{CA} *Pten*^{loxP} *Tyr::CreERT2* mice were topically applied on the skin with 2 µl of 25 mg/ml 4-hydroxytamoxifen (≥70% Z isomer, Sigma-Aldrich) dissolved in dimethyl sulfoxide (Sigma-Aldrich) on three consecutive days. Approximately 21 – 28 days later when tumor nodules have formed, mice were treated with IL-2cx or anti-PD-1 every other day, as described above (fig. 6F).

Cytokine measurements

Serum samples from mice were collected and stored at -80°C until cytokine testing. Serum cytokine concentrations were determined using Mouse GM-CSF ELISA MAX Standard (BioLegend), Mouse TNF-alpha Quantikine HS ELISA kit (R&D Systems) and Mouse Flt-3L ELISA Kit (Thermo Fisher Scientific). Measurements were performed in accordance to manufacturer's instructions.

Human serum samples before and after aldesleukin treatment were collected and stored as described before. GM-CSF was measured using Human GM-CSF ELISA MAX Standard (BioLegend). Human FLT3L and TNF were measured with proximity extension assay using the Olink Inflammation Panel.

Gene expression correlation analyses

For mouse *Il2r* expression analysis, RNA-seq and microarray data were retrieved from the ImmGen database (*40*) and plotted as relative expression in indicated immune cell subsets.

The RNA-seq data set for skin cutaneous melanoma was downloaded with Firebrowse (The Broad Institute) from The Cancer Genome Atlas (TCGA) (*67*). Gene expression was log2-transformed (log2[gene expression + 1]) and different genes of interest were correlated against each other. For gene signatures, the mean expression of all signature genes was calculated and plotted against *BATF3* expression. The NK cell signature was defined by the genes *NCR1, NCR3, KLRB1, CD160, and PRF1* (*15*). The IL-2 signature was defined by the IL-2-target genes *LTA*, *ARHGDIA*, *PKD2*, *LTB*, *KLF6*, *PDIA3*, *GZMB*, *PSMB1*, *S100A4*, and *FLT3LG* (*51*); and *IL2*. Significance of correlative

gene expression was calculated by using Pearson's correlation coefficient. Survival analysis was done with gene expression profiling interactive analysis 2 (*68*).

Quantitative polymerase chain reaction (qPCR)

RNA was isolated with the RNeasy Plus Micro and Mini Kits (Qiagen) from 250'000-1'000'000 FACS sorted cDCs ($CD3^-$ $CD19^-$ $NK1.1^-$ $CD45RB^-$ MHC-II^+ $CD11c^+$), $CD4^+$ conventional T (Tcon; $CD3^+$ $CD4^+$ $Foxp3^-$) and $CD4^+$ regulatory T cells (Treg; $CD3^+$ $CD4^+$ $Foxp3^+$) from *Foxp3*-GFP-DTR mice. Control RNA was isolated from untreated bulk wild-type, *Il2ra*$^{-/-}$, *Il2rb*$^{-/-}$, *and Il2rg*$^{-/-}$ splenocytes. After cDNA reverse transcription (High Capacity cDNA Reverse Transcription Kit, Applied Biosystems), qPCR analysis was performed using SYBR green (KAPA SYBR FAST, Roche) on a 7900HT Fast Real-Time PCR System (Applied Biosystems) and ΔΔCt values calculated. The following primer sequences were used:

Hprt (forward: GAT CAG TCA ACG GGG GAC AT, reverse: ATC CAA CAA AGT CTG GCC TGT),

Il2ra (forward: AAC CAT AGT ACC CAG TTG TCG G, reverse: TCC TAA GCA ACG CAT ATA GAC CA),

Il2rb (forward: TGG AGC CTG TCC CTC TAC G, reverse: TCC ACA TGC AAG AGA CAT TGG),

Il2rg (forward: GGT TAC TGA ATA CCA AGG GAA CTT T, reverse: TGG CAG AAC CGT TCA CTG TA).

RNA sequencing (RNA-seq)

Forty thousand splenic mouse cDCs from untreated and IL-2cx–treated wild-type mice were separated by FACS in RLT Plus lysis buffer (Qiagen) containing 1% 2-mercaptoethanol (Sigma-Aldrich). Subsequently, RNA was isolated using the RNeasy Plus Micro Kit (Qiagen). RNA-seq and data processing was done by the Functional Genomics Center Zurich, as briefly described here. The RNA extracted from sorted cells was quantified for quality and concentration using the TapeStation RNA high sensitivity kit (Agilent). The estimated RINs were in a range of 8.4 – 9.8 showing a good RNA quality; the RNA concentrations of 1.1 – 10 ng/µl recommended the use of a low input library preparation method. Accordingly, the SMARTer Stranded Total RNA Seq Kit v2 (Takara Bio) was used to prepare cDNA by universal priming (with 3 min fragmentation) and to deplete ribosomal cDNA with ZapR v2 and R Probes v2. The libraries were quantified by Tapestation D1000 (Agilent) measurements, and they showed fragment sizes around 320 bp. The libraries were sequenced on a HiSeq 4000 platform using 125 cycles single-read targeting ~40M reads per sample. Adapters and low-quality tails were trimmed from reads prior to read alignment. STAR aligner (v2.5.4b) (*69*) was used to align the RNA-seq dataset to Ensembl genome build GRCh38.p10 (Release 91). Gene expression counts were calculated with feature counts from Bioconductor package Rsubread (v1.32.1) (*70*). A gene was considered as expressed if, in at least one group of the comparison, it had more than 10 counts in more than half of the samples. Differentially expressed genes were detected using Bioconductor package EdgeR (v3.20.6) (*71*). Gene set enrichment analysis was done with Gene Ontology analyzer for RNA-seq and other length-biased data (goseq, v1.30.0)

(*72*). For the heatmap display, the top 75 up-regulated and top 75 down-regulated genes were log2-transformed (log2[normalized gene count + 1]) for calculation of Z-scores.

Software

Specific software used for analysis is mentioned where applied. Two cartoons were created using Biorender.com.

Statistical analyses

Detailed information on sample numbers and statistical tests used are described in the figure legends. Calculation was performed with the GraphPad Prism 8 software package. In general, differences between two groups were tested with t-tests for normally distributed data or Mann-Whitney test for not normally distributed data. Multiple comparison was done with either one-way ANOVA followed by Holm-Sidak's multiple comparison test for normally distributed data or Kruskall-Wallis test followed by Dunn's multiple comparison test for not normally distributed data. Time-dependent comparisons were tested with two-way ANOVA or mixed-effects model, followed by Holm-Sidak's multiple comparison test. Normality testing was done using d'Agostino-Pearson test. Correlation analysis was done with Pearson correlation coefficient and survival analysis with Logrank test. For all statistical analyses, significance was accepted at the 95% confidence level ($P < 0.05$). Exact *P*-values are provided; n.s. indicates not significant.

SUPPLEMENTARY MATERIALS

- Fig. S1. Different IL-2 formulations cause cDC1 and cDC2 expansion.
- Fig. S2. Apoptosis-mediating proteins in cDCs do not change after IL-2cx treatment.
- Fig. S3. IL-2 receptor (IL-2R) expression in stimulated cDCs and IL-2cx-treated cDCs and DC precursors.
- Fig. S4. Expansion of cDC subsets in *Flt3l*$^{-/-}$ *Csf2*$^{-/-}$ mice and cDC proliferation in etanercept-treated wild-type mice.
- Fig. S5. IL-2 receptor expression on different leukocytes and expansion of CD4^{+} T, CD8^{+} T and NK cells by IL-2 complexes.
- Fig. S6. DCs show improved antigen processing and facilitate anti-tumor responses after IL-2cx treatment.
- Fig. S7: Model of IL-2–mediated DC expansion and tumor infiltration.
- Table S1: Antibodies and fluorescent dyes used for flow cytometry.
- Data file S1: Primary data.

REFERENCES AND NOTES

1. R. M. Steinman, Decisions about dendritic cells: past, present, and future. *Annu Rev Immunol* **30**, 1-22 (2012).
2. A. Mildner, S. Jung, Development and function of dendritic cell subsets. *Immunity* **40**, 642-656 (2014).
3. V. Durai, K. M. Murphy, Functions of Murine Dendritic Cells. *Immunity* **45**, 719-736 (2016).
4. A. C. Villani, R. Satija, G. Reynolds, S. Sarkizova, K. Shekhar, J. Fletcher, M. Griesbeck, A. Butler, S. Zheng, S. Lazo, L. Jardine, D. Dixon, E. Stephenson, E. Nilsson, I. Grundberg, D. McDonald, A. Filby, W. Li, P. L. De Jager, O. Rozenblatt-Rosen *et al.*, Single-cell RNA-seq reveals new types of human blood dendritic cells, monocytes, and progenitors. *Science* **356**, eaah4573 (2017).
5. C. A. Dutertre, E. Becht, S. E. Irac, A. Khalilnezhad, V. Narang, S. Khalilnezhad, P. Y. Ng, L. L. van den Hoogen, J. Y. Leong, B. Lee, M. Chevrier, X. M. Zhang, P. J. A. Yong, G. Koh, J. Lum, S. W. Howland, E. Mok, J. Chen, A. Larbi, H. K. K. Tan *et al.*, Single-Cell Analysis of Human Mononuclear Phagocytes Reveals Subset-Defining Markers and Identifies Circulating Inflammatory Dendritic Cells. *Immunity* **51**, 573-589 e578 (2019).
6. B. U. Schraml, C. Reis e Sousa, Defining dendritic cells. *Curr Opin Immunol* **32**, 13-20 (2015).
7. T. Worbs, S. I. Hammerschmidt, R. Forster, Dendritic cell migration in health and disease. *Nat Rev Immunol* **17**, 30-48 (2017).

8. M. L. Broz, M. Binnewies, B. Boldajipour, A. E. Nelson, J. L. Pollack, D. J. Erle, A. Barczak, M. D. Rosenblum, A. Daud, D. L. Barber, S. Amigorena, L. J. Van't Veer, A. I. Sperling, D. M. Wolf, M. F. Krummel, Dissecting the tumor myeloid compartment reveals rare activating antigen-presenting cells critical for T cell immunity. *Cancer Cell* **26**, 638-652 (2014).
9. E. W. Roberts, M. L. Broz, M. Binnewies, M. B. Headley, A. E. Nelson, D. M. Wolf, T. Kaisho, D. Bogunovic, N. Bhardwaj, M. F. Krummel, Critical Role for CD103(+)/CD141(+) Dendritic Cells Bearing CCR7 for Tumor Antigen Trafficking and Priming of T Cell Immunity in Melanoma. *Cancer Cell* **30**, 324-336 (2016).
10. H. Salmon, J. Idoyaga, A. Rahman, M. Leboeuf, R. Remark, S. Jordan, M. Casanova-Acebes, M. Khudoynazarova, J. Agudo, N. Tung, S. Chakarov, C. Rivera, B. Hogstad, M. Bosenberg, D. Hashimoto, S. Gnjatic, N. Bhardwaj, A. K. Palucka, B. D. Brown, J. Brody *et al.*, Expansion and Activation of CD103(+) Dendritic Cell Progenitors at the Tumor Site Enhances Tumor Responses to Therapeutic PD-L1 and BRAF Inhibition. *Immunity* **44**, 924-938 (2016).
11. S. Spranger, D. Dai, B. Horton, T. F. Gajewski, Tumor-Residing Batf3 Dendritic Cells Are Required for Effector T Cell Trafficking and Adoptive T Cell Therapy. *Cancer Cell* **31**, 711-723 e714 (2017).
12. C. S. Garris, S. P. Arlauckas, R. H. Kohler, M. P. Trefny, S. Garren, C. Piot, C. Engblom, C. Pfirschke, M. Siwicki, J. Gungabeesoon, G. J. Freeman, S. E. Warren, S. Ong, E. Browning, C. G. Twitty, R. H. Pierce, M. H. Le, A. P. Algazi, A. I. Daud, S. I. Pai *et al.*, Successful Anti-PD-1 Cancer Immunotherapy Requires T Cell-

Dendritic Cell Crosstalk Involving the Cytokines IFN-gamma and IL-12. *Immunity* **49**, 1148-1161 e1147 (2018).

13. B. Ruffell, D. Chang-Strachan, V. Chan, A. Rosenbusch, C. M. Ho, N. Pryer, D. Daniel, E. S. Hwang, H. S. Rugo, L. M. Coussens, Macrophage IL-10 blocks CD8+ T cell-dependent responses to chemotherapy by suppressing IL-12 expression in intratumoral dendritic cells. *Cancer Cell* **26**, 623-637 (2014).
14. A. R. Sanchez-Paulete, F. J. Cueto, M. Martinez-Lopez, S. Labiano, A. Morales-Kastresana, M. E. Rodriguez-Ruiz, M. Jure-Kunkel, A. Azpilikueta, M. A. Aznar, J. I. Quetglas, D. Sancho, I. Melero, Cancer Immunotherapy with Immunomodulatory Anti-CD137 and Anti-PD-1 Monoclonal Antibodies Requires BATF3-Dependent Dendritic Cells. *Cancer Discov* **6**, 71-79 (2016).
15. J. P. Bottcher, E. Bonavita, P. Chakravarty, H. Blees, M. Cabeza-Cabrerizo, S. Sammicheli, N. C. Rogers, E. Sahai, S. Zelenay, C. Reis e Sousa, NK Cells Stimulate Recruitment of cDC1 into the Tumor Microenvironment Promoting Cancer Immune Control. *Cell* **172**, 1022-1037 e1014 (2018).
16. K. C. Barry, J. Hsu, M. L. Broz, F. J. Cueto, M. Binnewies, A. J. Combes, A. E. Nelson, K. Loo, R. Kumar, M. D. Rosenblum, M. D. Alvarado, D. M. Wolf, D. Bogunovic, N. Bhardwaj, A. I. Daud, P. K. Ha, W. R. Ryan, J. L. Pollack, B. Samad, S. Asthana *et al.*, A natural killer-dendritic cell axis defines checkpoint therapy-responsive tumor microenvironments. *Nat Med* **24**, 1178-1191 (2018).
17. M. E. Raeber, Y. Zurbuchen, D. Impellizzieri, O. Boyman, The role of cytokines in T-cell memory in health and disease. *Immunol Rev* **283**, 176-193 (2018).

18. W. J. Leonard, J. X. Lin, J. J. O'Shea, The gammac Family of Cytokines: Basic Biology to Therapeutic Ramifications. *Immunity* **50**, 832-850 (2019).
19. N. Arenas-Ramirez, J. Woytschak, O. Boyman, Interleukin-2: Biology, Design and Application. *Trends Immunol* **36**, 763-777 (2015).
20. T. R. Malek, I. Castro, Interleukin-2 receptor signaling: at the interface between tolerance and immunity. *Immunity* **33**, 153-165 (2010).
21. A. K. Abbas, E. Trotta, R. S. D, A. Marson, J. A. Bluestone, Revisiting IL-2: Biology and therapeutic prospects. *Sci Immunol* **3**, eaat1482 (2018).
22. S. Letourneau, E. M. van Leeuwen, C. Krieg, C. Martin, G. Pantaleo, J. Sprent, C. D. Surh, O. Boyman, IL-2/anti-IL-2 antibody complexes show strong biological activity by avoiding interaction with IL-2 receptor alpha subunit CD25. *Proc Natl Acad Sci U S A* **107**, 2171-2176 (2010).
23. C. Krieg, S. Letourneau, G. Pantaleo, O. Boyman, Improved IL-2 immunotherapy by selective stimulation of IL-2 receptors on lymphocytes and endothelial cells. *Proc Natl Acad Sci U S A* **107**, 11906-11911 (2010).
24. N. Arenas-Ramirez, C. Zou, S. Popp, D. Zingg, B. Brannetti, E. Wirth, T. Calzascia, J. Kovarik, L. Sommer, G. Zenke, J. Woytschak, C. H. Regnier, A. Katopodis, O. Boyman, Improved cancer immunotherapy by a CD25-mimobody conferring selectivity to human interleukin-2. *Sci Transl Med* **8**, 367ra166 (2016).
25. D. Klatzmann, A. K. Abbas, The promise of low-dose interleukin-2 therapy for autoimmune and inflammatory diseases. *Nat Rev Immunol* **15**, 283-294 (2015).
26. J. Y. Humrich, C. von Spee-Mayer, E. Siegert, M. Bertolo, A. Rose, D. Abdirama, P. Enghard, B. Stuhlmüller, B. Sawitzki, D. Huscher, F. Hiepe, T. Alexander, E. Feist,

A. Radbruch, G.-R. Burmester, G. Riemekasten, Low-dose interleukin-2 therapy in refractory systemic lupus erythematosus: an investigator-initiated, single-centre phase 1 and 2a clinical trial. *The Lancet Rheumatology* **1**, e44-e54 (2019).

27. M. Rapp, M. W. M. Wintergerst, W. G. Kunz, V. K. Vetter, M. M. L. Knott, D. Lisowski, S. Haubner, S. Moder, R. Thaler, S. Eiber, B. Meyer, N. Rohrle, I. Piseddu, S. Grassmann, P. Layritz, B. Kuhnemuth, S. Stutte, C. Bourquin, U. H. von Andrian, S. Endres *et al.*, CCL22 controls immunity by promoting regulatory T cell communication with dendritic cells in lymph nodes. *J Exp Med* **216**, 1170-1181 (2019).
28. M. Merad, P. Sathe, J. Helft, J. Miller, A. Mortha, The dendritic cell lineage: ontogeny and function of dendritic cells and their subsets in the steady state and the inflamed setting. *Annu Rev Immunol* **31**, 563-604 (2013).
29. V. Durai, P. Bagadia, J. M. Granja, A. T. Satpathy, D. H. Kulkarni, J. T. t. Davidson, R. Wu, S. J. Patel, A. Iwata, T. T. Liu, X. Huang, C. G. Briseno, G. E. Grajales-Reyes, M. Wohner, H. Tagoh, B. L. Kee, R. D. Newberry, M. Busslinger, H. Y. Chang, T. L. Murphy *et al.*, Cryptic activation of an Irf8 enhancer governs cDC1 fate specification. *Nat Immunol* **20**, 1161-1173 (2019).
30. P. Bagadia, X. Huang, T. T. Liu, V. Durai, G. E. Grajales-Reyes, M. Nitschke, Z. Modrusan, J. M. Granja, A. T. Satpathy, C. G. Briseno, M. Gargaro, A. Iwata, S. Kim, H. Y. Chang, A. S. Shaw, T. L. Murphy, K. M. Murphy, An Nfil3-Zeb2-Id2 pathway imposes Irf8 enhancer switching during cDC1 development. *Nat Immunol* **20**, 1174-1185 (2019).

31. D. K. Fogg, C. Sibon, C. Miled, S. Jung, P. Aucouturier, D. R. Littman, A. Cumano, F. Geissmann, A clonogenic bone marrow progenitor specific for macrophages and dendritic cells. *Science* **311**, 83-87 (2006).
32. N. Onai, A. Obata-Onai, M. A. Schmid, T. Ohteki, D. Jarrossay, M. G. Manz, Identification of clonogenic common Flt3+M-CSFR+ plasmacytoid and conventional dendritic cell progenitors in mouse bone marrow. *Nat Immunol* **8**, 1207-1216 (2007).
33. M. G. Manz, S. Boettcher, Emergency granulopoiesis. *Nat Rev Immunol* **14**, 302-314 (2014).
34. S. Shalini, L. Dorstyn, S. Dawar, S. Kumar, Old, new and emerging functions of caspases. *Cell Death Differ* **22**, 526-539 (2015).
35. J. M. Adams, S. Cory, The Bcl-2 apoptotic switch in cancer development and therapy. *Oncogene* **26**, 1324-1337 (2007).
36. C. Pilon, B. Levast, F. Meurens, Y. Le Vern, D. Kerboeuf, H. Salmon, F. Velge-Roussel, Y. Lebranchu, C. Baron, CD40 engagement strongly induces CD25 expression on porcine dendritic cells and polarizes the T cell immune response toward Th1. *Mol Immunol* **46**, 437-447 (2009).
37. J. Obendorf, P. Renner Viveros, M. Fehlings, C. Klotz, T. Aebischer, R. Ignatius, Increased expression of CD25, CD83, and CD86, and secretion of IL-12, IL-23, and IL-10 by human dendritic cells incubated in the presence of Toll-like receptor 2 ligands and Giardia duodenalis. *Parasit Vectors* **6**, 317 (2013).
38. M. Merad, M. G. Manz, Dendritic cell homeostasis. *Blood* **113**, 3418-3427 (2009).

39. D. Zingg, N. Arenas-Ramirez, D. Sahin, R. A. Rosalia, A. T. Antunes, J. Haeusel, L. Sommer, O. Boyman, The Histone Methyltransferase Ezh2 Controls Mechanisms of Adaptive Resistance to Tumor Immunotherapy. *Cell Rep* **20**, 854-867 (2017).

40. T. S. Heng, M. W. Painter, C. Immunological Genome Project, The Immunological Genome Project: networks of gene expression in immune cells. *Nat Immunol* **9**, 1091-1094 (2008).

41. O. Boyman, M. Kovar, M. P. Rubinstein, C. D. Surh, J. Sprent, Selective stimulation of T cell subsets with antibody-cytokine immune complexes. *Science* **311**, 1924-1927 (2006).

42. A. M. Levin, D. L. Bates, A. M. Ring, C. Krieg, J. T. Lin, L. Su, I. Moraga, M. E. Raeber, G. R. Bowman, P. Novick, V. S. Pande, C. G. Fathman, O. Boyman, K. C. Garcia, Exploiting a natural conformational switch to engineer an interleukin-2 'superkine'. *Nature* **484**, 529-533 (2012).

43. J. K. Bando, M. Colonna, Innate lymphoid cell function in the context of adaptive immunity. *Nat Immunol* **17**, 783-789 (2016).

44. A. V. Villarino, G. Sciume, F. P. Davis, S. Iwata, B. Zitti, G. W. Robinson, L. Hennighausen, Y. Kanno, J. J. O'Shea, Subset- and tissue-defined STAT5 thresholds control homeostasis and function of innate lymphoid cells. *J Exp Med* **214**, 2999-3014 (2017).

45. C. Seillet, L. A. Mielke, D. B. Amann-Zalcenstein, S. Su, J. Gao, F. F. Almeida, W. Shi, M. E. Ritchie, S. H. Naik, N. D. Huntington, S. Carotta, G. T. Belz, Deciphering the Innate Lymphoid Cell Transcriptional Program. *Cell Rep* **17**, 436-447 (2016).

46. M. Binnewies, A. M. Mujal, J. L. Pollack, A. J. Combes, E. A. Hardison, K. C. Barry, J. Tsui, M. K. Ruhland, K. Kersten, M. A. Abushawish, M. Spasic, J. P. Giurintano, V. Chan, A. I. Daud, P. Ha, C. J. Ye, E. W. Roberts, M. F. Krummel, Unleashing Type-2 Dendritic Cells to Drive Protective Antitumor CD4(+) T Cell Immunity. *Cell* **177**, 556-571 (2019).
47. R. Sporri, C. Reis e Sousa, Inflammatory mediators are insufficient for full dendritic cell activation and promote expansion of CD4+ T cell populations lacking helper function. *Nat Immunol* **6**, 163-170 (2005).
48. R. A. Rosalia, E. D. Quakkelaar, A. Redeker, S. Khan, M. Camps, J. W. Drijfhout, A. L. Silva, W. Jiskoot, T. van Hall, P. A. van Veelen, G. Janssen, K. Franken, L. J. Cruz, A. Tromp, J. Oostendorp, S. H. van der Burg, F. Ossendorp, C. J. Melief, Dendritic cells process synthetic long peptides better than whole protein, improving antigen presentation and T-cell activation. *Eur J Immunol* **43**, 2554-2565 (2013).
49. M. Sharma, H. Khong, F. Fa'ak, S. E. Bentebibel, L. M. E. Janssen, B. C. Chesson, C. A. Creasy, M. A. Forget, L. M. S. Kahn, B. Pazdrak, B. Karki, Y. Hailemichael, M. Singh, C. Vianden, S. Vennam, U. Bharadwaj, D. J. Tweardy, C. Haymaker, C. Bernatchez, S. Huang *et al.*, Bempegaldesleukin selectively depletes intratumoral Tregs and potentiates T cell-mediated cancer therapy. *Nat Commun* **11**, 661 (2020).
50. O. A. Ali, S. A. Lewin, G. Dranoff, D. J. Mooney, Vaccines Combined with Immune Checkpoint Antibodies Promote Cytotoxic T-cell Activity and Tumor Eradication. *Cancer Immunol Res* **4**, 95-100 (2016).
51. P. E. Kovanen, L. Young, A. Al-Shami, V. Rovella, C. A. Pise-Masison, M. F. Radonovich, J. Powell, J. Fu, J. N. Brady, P. J. Munson, W. J. Leonard, Global

analysis of IL-2 target genes: identification of chromosomal clusters of expressed genes. *Int Immunol* **17**, 1009-1021 (2005).

52. J. M. Trevejo, M. W. Marino, N. Philpott, R. Josien, E. C. Richards, K. B. Elkon, E. Falck-Pedersen, TNF-alpha -dependent maturation of local dendritic cells is critical for activating the adaptive immune response to virus infection. *Proc Natl Acad Sci U S A* **98**, 12162-12167 (2001).
53. P. Chomarat, C. Dantin, L. Bennett, J. Banchereau, A. K. Palucka, TNF skews monocyte differentiation from macrophages to dendritic cells. *J Immunol* **171**, 2262-2269 (2003).
54. A. D. Guerrero, M. B. Dong, Y. Zhao, A. Lau-Kilby, K. V. Tarbell, Interleukin-2-mediated inhibition of dendritic cell development correlates with decreased CD135 expression and increased monocyte/macrophage precursors. *Immunology* **143**, 640-650 (2014).
55. A. W. Lau-Kilby, C. C. Kretz, S. Pechhold, J. D. Price, S. Dorta, H. Ramos, G. Trinchieri, K. V. Tarbell, Interleukin-2 inhibits FMS-like tyrosine kinase 3 receptor ligand (flt3L)-dependent development and function of conventional and plasmacytoid dendritic cells. *Proc Natl Acad Sci U S A* **108**, 2408-2413 (2011).
56. V. Kronin, D. Vremec, K. Shortman, Does the IL-2 receptor alpha chain induced on dendritic cells have a biological function? *Int Immunol* **10**, 237-240 (1998).
57. T. Fukao, S. Koyasu, Expression of functional IL-2 receptors on mature splenic dendritic cells. *Eur J Immunol* **30**, 1453-1457 (2000).

58. F. W. Velten, F. Rambow, P. Metharom, S. Goerdt, Enhanced T-cell activation and T-cell-dependent IL-2 production by CD83+, CD25high, CD43high human monocyte-derived dendritic cells. *Mol Immunol* **44**, 1544-1550 (2007).
59. M. Crowley, K. Inaba, M. Witmer-Pack, R. M. Steinman, The cell surface of mouse dendritic cells: FACS analyses of dendritic cells from different tissues including thymus. *Cell Immunol* **118**, 108-125 (1989).
60. P. S. Freudenthal, R. M. Steinman, The distinct surface of human blood dendritic cells, as observed after an improved isolation method. *Proc Natl Acad Sci U S A* **87**, 7698-7702 (1990).
61. O. Boyman, J. Sprent, The role of interleukin-2 during homeostasis and activation of the immune system. *Nat Rev Immunol* **12**, 180-190 (2012).
62. S. C. Wuest, J. H. Edwan, J. F. Martin, S. Han, J. S. Perry, C. M. Cartagena, E. Matsuura, D. Maric, T. A. Waldmann, B. Bielekova, A role for interleukin-2 trans-presentation in dendritic cell-mediated T cell activation in humans, as revealed by daclizumab therapy. *Nat Med* **17**, 604-609 (2011).
63. A. Diab, M. E. Hurwitz, D. C. Cho, V. Papadimitrakopoulou, B. D. Curti, S. S. Tykodi, I. Puzanov, N. K. Ibrahim, S. M. Tolaney, D. Tripathy, J. Gao, A. O. Siefker-Radtke, W. Clemens, M. A. Tagliaferri, S. N. Gettinger, H. M. Kluger, J. M. G. Larkin, G. Grignani, M. Sznol, N. M. Tannir, NKTR-214 (CD122-biased agonist) plus nivolumab in patients with advanced solid tumors: Preliminary phase 1/2 results of PIVOT. *J Clin Oncol* **36**, 3006-3006 (2018).
64. S. A. Rosenberg, IL-2: the first effective immunotherapy for human cancer. *J Immunol* **192**, 5451-5458 (2014).

65. M. A. Williams, M. J. Bevan, Effector and memory CTL differentiation. *Annu Rev Immunol* **25**, 171-192 (2007).

66. O. Boyman, J. H. Cho, J. T. Tan, C. D. Surh, J. Sprent, A major histocompatibility complex class I-dependent subset of memory phenotype CD8+ cells. *J Exp Med* **203**, 1817-1825 (2006).

67. N. Cancer Genome Atlas, Genomic Classification of Cutaneous Melanoma. *Cell* **161**, 1681-1696 (2015).

68. Z. Tang, B. Kang, C. Li, T. Chen, Z. Zhang, GEPIA2: an enhanced web server for large-scale expression profiling and interactive analysis. *Nucleic Acids Res* **47**, W556-W560 (2019).

69. A. Dobin, C. A. Davis, F. Schlesinger, J. Drenkow, C. Zaleski, S. Jha, P. Batut, M. Chaisson, T. R. Gingeras, STAR: ultrafast universal RNA-seq aligner. *Bioinformatics* **29**, 15-21 (2013).

70. Y. Liao, G. K. Smyth, W. Shi, The Subread aligner: fast, accurate and scalable read mapping by seed-and-vote. *Nucleic Acids Res* **41**, e108 (2013).

71. M. D. Robinson, D. J. McCarthy, G. K. Smyth, edgeR: a Bioconductor package for differential expression analysis of digital gene expression data. *Bioinformatics* **26**, 139-140 (2010).

72. M. D. Young, M. J. Wakefield, G. K. Smyth, A. Oshlack, Gene ontology analysis for RNA-seq: accounting for selection bias. *Genome Biol* **11**, R14 (2010).

ACKNOWLEDGMENTS

We thank Laura Bürgi for help with experiments, Urs Steiner, Elisabeth Käser and Corina Defila for their support with the clinical trial, Yves Zurbuchen and Carlo Cervia for their support in maintaining the mouse colony during the SARS-CoV-2 pandemic, Markus Manz (University Hospital Zurich) and Antonios Rolink (University of Basel) for providing mice, and the members of the Boyman laboratory for discussion and critical reading of the manuscript. Editorial services were provided by Nancy R. Gough (BioSerendipity, LLC, Elkridge, MD).

FUNDING

This work was supported by the Swiss National Science Foundation (310030-172978; to O.B.), the Hochspezialisierte Medizin Schwerpunkt Immunologie (HSM-2-Immunologie; to O.B.), the Clinical Research Priority Program CYTIMM-Z of the University of Zurich (to O.B.), Swiss Cancer Research grant (KFS-4136-02-2017; to O.B.), Swiss Cancer MD-PhD fellowship (MD-PhD-3557-06-2015; to M.R.), Fritz Rohrer-Fonds (to M.R. and O.B.), Olga Mayenfisch Stiftung (to M.R.), EMDO Stiftung (to M.R. and O.B.), and the Young Talents in Clinical Research Fellowship by the Swiss Academy of Medical Sciences and Bangerter Foundation (YTCR 32/18, to M.R.).

AUTHOR CONTRIBUTIONS

M.R. designed and performed experiments, conducted the clinical trial, analyzed the data and wrote the manuscript. R.A.R. designed and performed experiments and gave scientific input. D.S. and U.K. performed experiments. O.B. designed and analyzed experiments,

supervised the study and the clinical trial, and wrote the manuscript with input from all the authors.

COMPETING INTERESTS

O.B. is a founder and shareholder of Anaveon AG, and holds patents on improved IL-2 formulations (patents WO2017122130A1, WO2014100014A1, WO2016005950A1, and WO2017121758A1). M.E.R., U.K., and O.B. are listed as inventors on a patent application on the use of IL-2 formulations for DC immunotherapy. The other authors declare that they have no competing interests.

DATA AND MATERIALS AVAILABILITY

The raw dataset generated by RNA-sequencing has been deposited in the ArrayExpress database at EMBL-EBI (www.ebi.ac.uk/arrayexpress) under accession number E-MTAB-8991. All other data and materials are available upon request from the corresponding author.

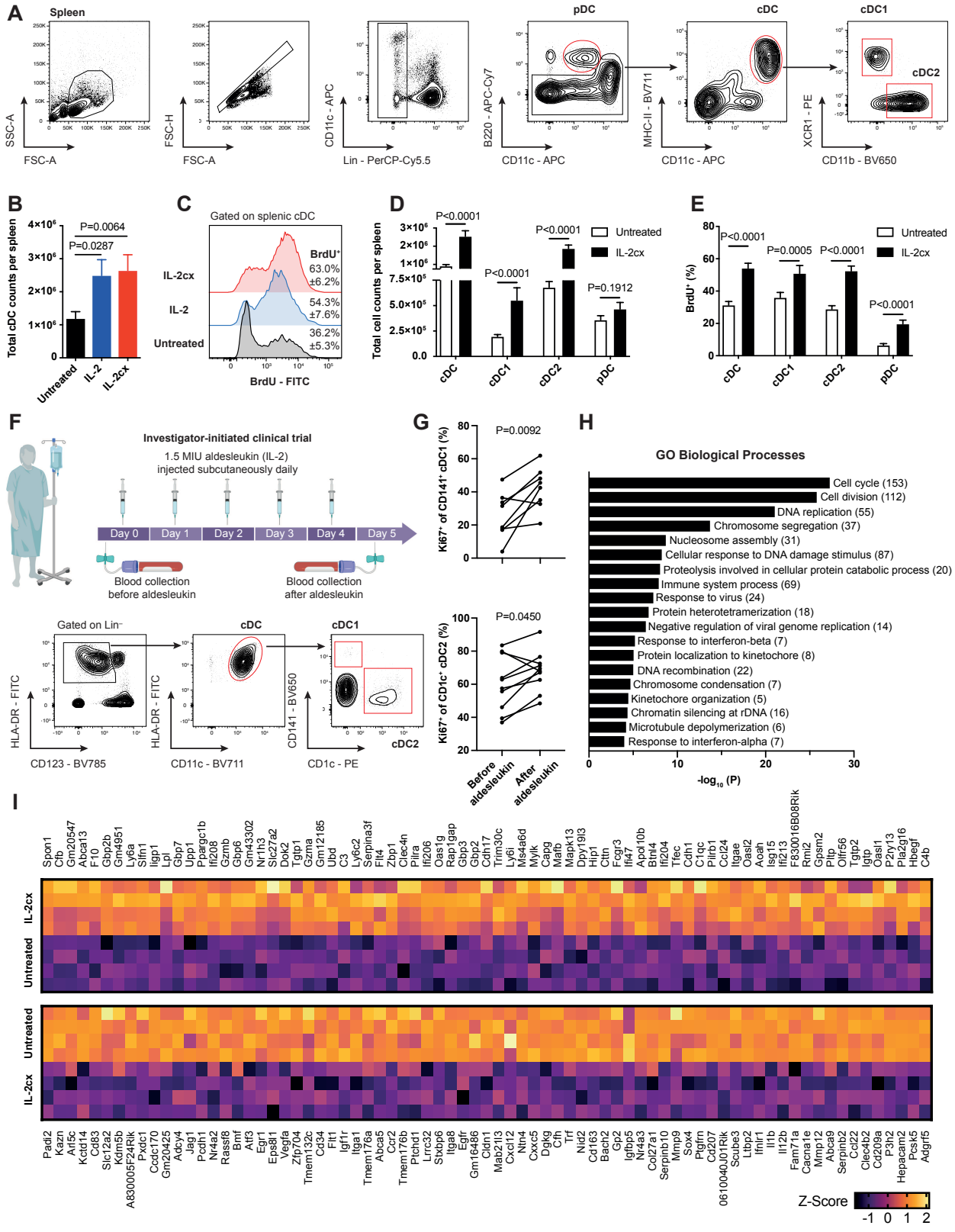
A
Spleen
SSC-A
FSC-A
FSC-H
FSC-A
CD11c - APC
Lin - PerCP-Cy5.5
pDC
cDC
cDC1
cDC2
B220 - APC-Cy7
CD11c - APC
MHC-II - BV711
CD11c - APC
XCR1 - PE
CD11b - BV650
B
Total cDC counts per spleen
P=0.0064
P=0.0287
Untreated
IL-2
IL-2cx
C
Gated on splenic cDC
IL-2cx
IL-2
Untreated
BrdU⁺
63.0%
±6.2%
54.3%
±7.6%
36.2%
±5.3%
BrdU - FITC
D
Total cell counts per spleen
P<0.0001
P<0.0001
P<0.0001
P=0.1912
Untreated
IL-2cx
cDC
cDC1
cDC2
pDC
E
BrdU⁺ (%)
P<0.0001
P=0.0005
P<0.0001
P<0.0001
Untreated
IL-2cx
cDC
cDC1
cDC2
pDC
F
Investigator-initiated clinical trial
1.5 MIU aldesleukin (IL-2)
injected subcutaneously daily
Day 0
Day 1
Day 2
Day 3
Day 4
Day 5
Blood collection
before aldesleukin
Blood collection
after aldesleukin
Gated on Lin⁻
cDC
cDC1
HLA-DR - FITC
CD123 - BV785
HLA-DR - FITC
CD11c - BV711
CD141 - BV650
CD1c - PE
cDC2
G
Ki67⁺ of CD141⁺ cDC1 (%)
P=0.0092
Ki67⁺ of CD1c⁺ cDC2 (%)
P=0.0450
Before aldesleukin
After aldesleukin
H
GO Biological Processes
Cell cycle (153)
Cell division (112)
DNA replication (55)
Chromosome segregation (37)
Nucleosome assembly (31)
Cellular response to DNA damage stimulus (87)
Proteolysis involved in cellular protein catabolic process (20)
Immune system process (69)
Response to virus (24)
Protein heterotetramerization (18)
Negative regulation of viral genome replication (14)
Response to interferon-beta (7)
Protein localization to kinetochore (8)
DNA recombination (22)
Chromosome condensation (7)
Kinetochore organization (5)
Chromatin silencing at rDNA (16)
Microtubule depolymerization (6)
Response to interferon-alpha (7)
-log10 (P)
I
IL-2cx
Untreated
Untreated
IL-2cx
Z-Score
-1 0 1 2

Figure 1

FIGURE LEGENDS

Fig. 1. IL-2 immunotherapy expands cDCs in mice and humans.

(**A**) Representative gating strategy for mouse splenic DC subsets including plasmacytoid DCs (pDC) and conventional type I and type II DCs (cDC1 and cDC2). (**B**) Total splenic cDC counts after treatment with IL-2 or IL-2 complexes (IL-2cx) in wild-type (WT) mice. Data are presented as mean +/- SEM (n = 7 to 9 mice per group from N = 3 independent experiments). (**C**) Proliferation of splenic cDCs from mice receiving the indicated treatments was measured by bromodeoxyuridine (BrdU) incorporation over 3 days. Data are presented as mean +/- SEM (n = 7 mice per group from N = 3 independent experiments). (**D** and **E**) Quantification of total numbers (D) and proliferation (E) of splenic cDC subsets from mice receiving the indicated treatments. Data are presented as mean +/- SEM (n = 19 (D) and 16 (E) mice per group from N = 8 (D) and 6 (E) independent experiments). (**F**) Study design of the investigator-initiated clinical trial testing 1.5 million international units (MIU) aldesleukin (recombinant human IL-2) injected subcutaneously daily on 5 consecutive days with blood draws before and after aldesleukin injection (upper panel). Corresponding gating strategy of human cDC subsets identifying $CD141^+$ cDC1 and $CD1c^+$ cDC2 (lower panel). (**G**) Percentages of $Ki67^+$ proliferating cDC1 (n = 8) and cDC2 (n = 10) in peripheral blood from patients before and after aldesleukin treatment. (**H**) Biological processes Gene Ontology (GO) terms enriched in RNA-seq data of IL-2cx-treated WT mice compared to untreated mice (n = 4 mice per group from 1 experiment). The numbers in parentheses refer to the count of significantly upregulated genes within each GO term. (**I**) Top 75 upregulated (top panel) and top 75 downregulated (bottom panel) genes in IL-2cx-treated WT mice compared to untreated mice. P-values calculated with

Kruskall-Wallis test with Dunn's multiple comparison test (B), Mann-Whitney test (D and E) or paired t-test (G).

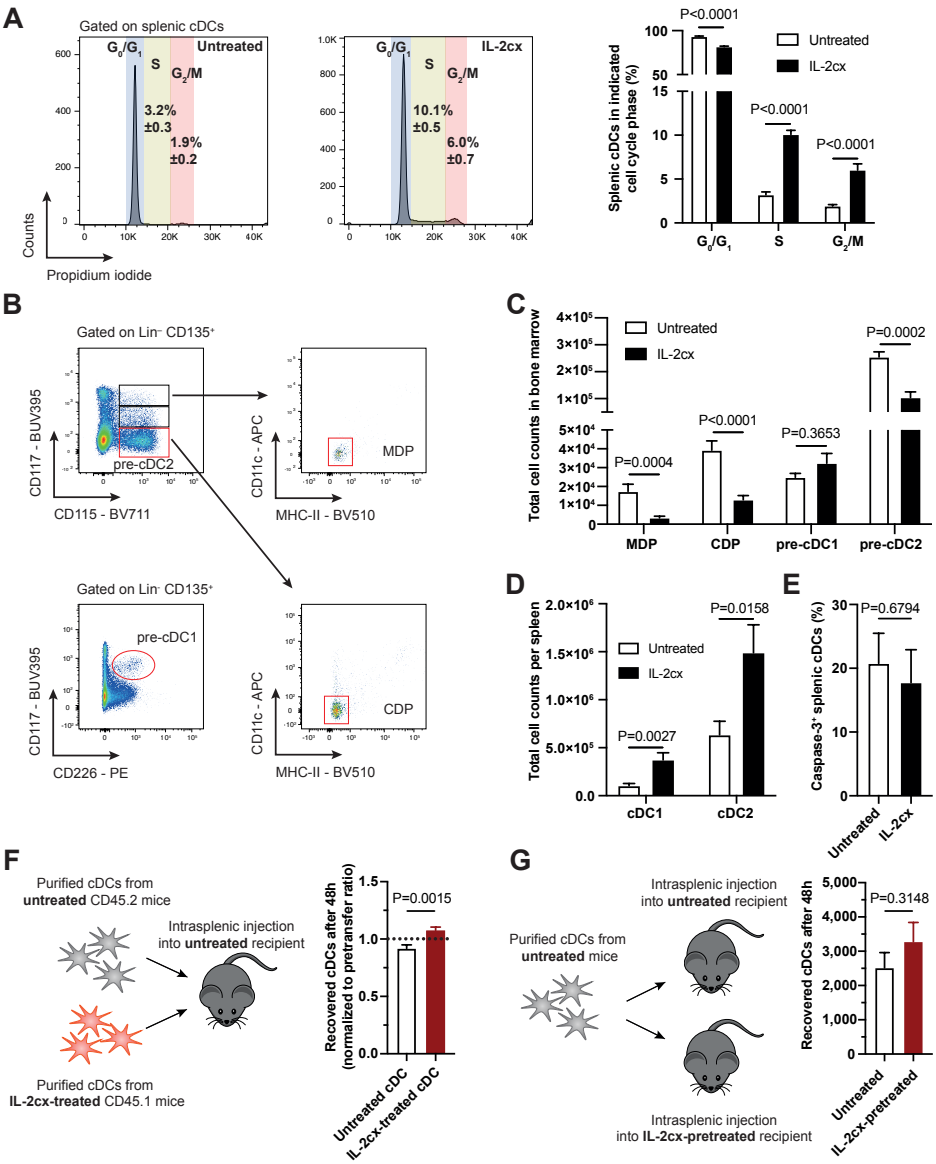
A
Gated on splenic cDCs
Untreated
IL-2cx
G0/G1
S
G2/M
3.2% ±0.3
1.9% ±0.2
10.1% ±0.5
6.0% ±0.7
Counts
Propidium iodide
Splenic cDCs in indicated cell cycle phase (%)
P<0.0001
P<0.0001
P<0.0001
B
Gated on Lin⁻ CD135⁺
CD117 - BUV395
CD115 - BV711
pre-cDC2
CD11c - APC
MHC-II - BV510
MDP
Gated on Lin⁻ CD135⁺
pre-cDC1
CD226 - PE
CDP
C
Total cell counts in bone marrow
P=0.0004
P<0.0001
P=0.3653
P=0.0002
MDP
CDP
pre-cDC1
pre-cDC2
D
Total cell counts per spleen
P=0.0027
P=0.0158
cDC1
cDC2
E
Caspase-3⁺ splenic cDCs (%)
P=0.6794
Untreated
IL-2cx
F
Purified cDCs from untreated CD45.2 mice
Intrasplenic injection into untreated recipient
Purified cDCs from IL-2cx-treated CD45.1 mice
Recovered cDCs after 48h (normalized to pretransfer ratio)
P=0.0015
Untreated cDC
IL-2cx-treated cDC
G
Purified cDCs from untreated mice
Intrasplenic injection into untreated recipient
Intrasplenic injection into IL-2cx-pretreated recipient
Recovered cDCs after 48h
P=0.3148
Untreated
IL-2cx-pretreated

Figure 2

Fig. 2. IL-2 causes proliferation of mature cDCs and differentiation of DC precursors. (**A**) Cell cycle analysis of splenic cDCs from IL-2cx-treated and untreated wild-type mice with the Watson model for cell cycle analysis for each cell cycle state including gap 0 (G0), gap 1 (G1), synthesis (S), gap 2 (G2), and mitosis (M). Data are presented as mean +/- SEM (n = 7 mice per group from N = 3 independent experiments). (**B**) Representative pseudocolor plots of bone marrow cells from untreated mice showing gating strategy for identifying monocyte/DC progenitor (MDP) cells, common dendritic cell progenitor (CDP) cells, precursor (pre)-cDC1, and pre-cDC2. (**C**) Total counts of precursor populations in bone marrow cells in mice receiving indicated treatments. Data are presented as mean +/- SEM (n = 11 mice per group from N = 3 independent experiments). (**D**) Total cell counts of splenic cDC1 and cDC2 from matched mice described in (C). Data are presented as mean +/- SEM (n = 11 mice per group from N = 3 independent experiments). (**E**) Activated caspase-3 in cDCs from untreated and IL-2cx–treated mice. Data are presented as mean +/- SEM (n = 4 to 5 mice per group from N = 2 independent experiments). (**F**) Survival of mature cDCs 48 hours after adoptive transfer of cDCs from both untreated and IL-2cx–treated donors into untreated recipient mice by intrasplenic injection. Data are presented as mean +/- SEM (n = 10 mice per group from N = 4 independent experiments). (**G**) Survival of mature cDCs 48 hours after adoptive transfer by intrasplenic injection of cDCs from untreated donor into either untreated or IL-2cx-pretreated recipient mice. Data are presented as mean +/- SEM (n = 8 to 9 mice per group from N = 2 independent experiments). P-values were calculated using multiple t-tests (A and D), Mann-Whitney test (C) or unpaired t-test (E to G).

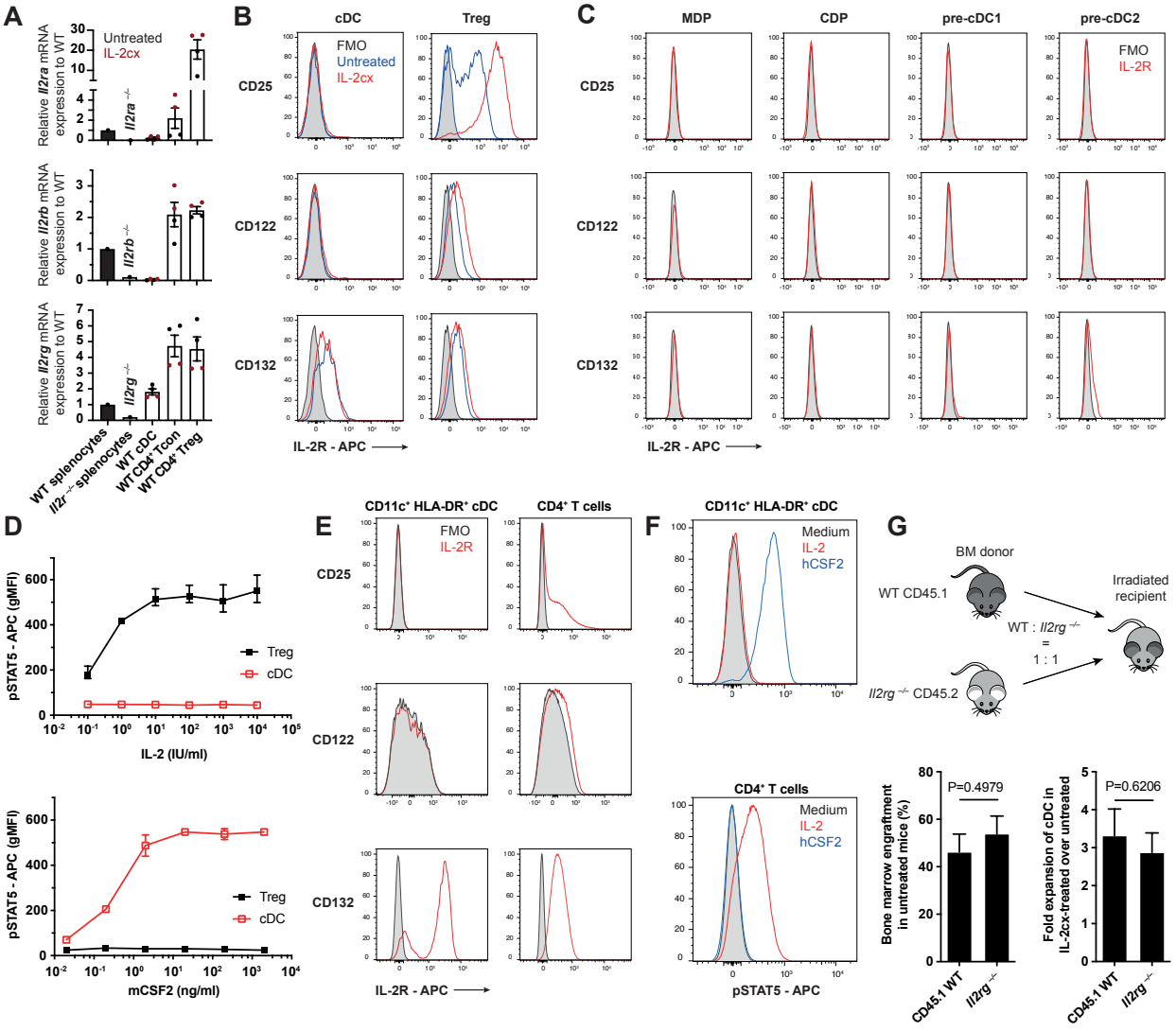
A
Relative Il2ra mRNA expression to WT
Untreated
IL-2cx
Il2ra -/-
Relative Il2rb mRNA expression to WT
Il2rb -/-
Relative Il2rg mRNA expression to WT
Il2rg -/-
WT splenocytes
Il2rg -/- splenocytes
WT cDC
WT CD4+ Tcon
WT CD4+ Treg
B
cDC
Treg
CD25
CD122
CD132
FMO
Untreated
IL-2cx
IL-2R - APC
C
MDP
CDP
pre-cDC1
pre-cDC2
CD25
CD122
CD132
FMO
IL-2R
IL-2R - APC
D
pSTAT5 - APC (gMFI)
Treg
cDC
IL-2 (IU/ml)
pSTAT5 - APC (gMFI)
Treg
cDC
mCSF2 (ng/ml)
E
CD11c+ HLA-DR+ cDC
CD4+ T cells
CD25
CD122
CD132
FMO
IL-2R
IL-2R - APC
F
CD11c+ HLA-DR+ cDC
Medium
IL-2
hCSF2
CD4+ T cells
Medium
IL-2
hCSF2
pSTAT5 - APC
G
BM donor
WT CD45.1
Irradiated recipient
WT : Il2rg -/-
=
1 : 1
Il2rg -/- CD45.2
Bone marrow engraftment in untreated mice (%)
P=0.4979
CD45.1 WT
Il2rg -/-
Fold expansion of cDC in IL-2cx-treated over untreated
P=0.6206
CD45.1 WT
Il2rg -/-

Figure 3

Fig. 3. Mature DCs and their precursors lack functional IL-2Rs.

(**A**) Relative mRNA expression of *Il2ra* (encoding CD25), *Il2rb* (CD122), and *Il2rg* (CD132) in cDCs from untreated (black dots) and IL-2cx-treated (red dots) mice compared to the expression in conventional T (Tcon) and regulatory T (Treg) cells from the same mice (n = 2 mice per group and treatment condition). Control conditions included splenocytes isolated from untreated wild-type (WT), *Il2ra*$^{-/-}$, *Il2rb*$^{-/-}$, and *Il2rg*$^{-/-}$ mice (n = 1 mouse per group). Data are presented as mean +/- SEM (N = 1 independent experiment with 4 technical replicates per mouse). (**B**) IL-2R subunit abundance on the surface of mouse splenic cDCs (left panel) and Treg cells (right panel) by flow cytometry. Displayed are representative histograms from n = 9 mice and N = 3 independent experiments showing the intensity of IL-2R subunit staining in untreated (blue line) and IL-2cx-treated (red line) mice, and the fluorescence minus one (FMO) control (grey shaded area). (**C**) IL-2R subunit abundance on the surface of DC precursors in bone marrow. MDP, monocyte/DC progenitor; CDP, common DC progenitor; pre-cDC1, precursor cDC1; pre-cDC2, precursor cDC2. Shown are representative histograms from n = 9 mice and N = 3 independent experiments showing the intensity of IL-2R subunit staining (red line) and FMO control (grey shaded area). (**D**) Phosphorylation of signal transducer and activator of transcription (STAT) 5 in mouse cDCs (red line) and Treg cells (black line) upon incubation with titrated concentrations of IL-2 (upper panel) or mouse CSF2 (mCSF2; lower panel). Data are presented as mean +/- SD (n = 2) from one of 3 independent experiments. (**E**) IL-2R subunit abundance on human CD11c$^+$ HLA-DR$^+$ cDCs compared to the abundance on CD4$^+$ T cells. Shown are representative histograms from 6 individual donors and N = 3 independent experiments of the respective intensity of IL-2R subunit

staining (red line) and FMO control (grey shaded area). (**F**) Evaluation of cytokine signaling by measurement of phosphorylated STAT5 (pSTAT5) in human cDCs and $CD4^+$ T cells after incubation with either IL-2 (red line, 1,000 IU/ml) or human CSF2 (hCSF2, blue line, 200 ng/ml). Shown are representative histograms from 6 individual donors and $N = 3$ independent experiments of the respective intensity of pSTAT5 staining and FMO control (grey shaded area). (**G**) Lethally-irradiated *Il2rg*$^{-/-}$ mice reconstituted with a 1:1-mix of $CD45.1^+$ WT and $CD45.2^+$ *Il2rg*$^{-/-}$ bone marrow cells receiving indicated treatments two months after reconstitution. Data are presented as mean +/- SEM ($n = 5$ to 9 mice per group from $N = 3$ independent experiments). BM, bone marrow. *P*-values were calculated using unpaired t-test.

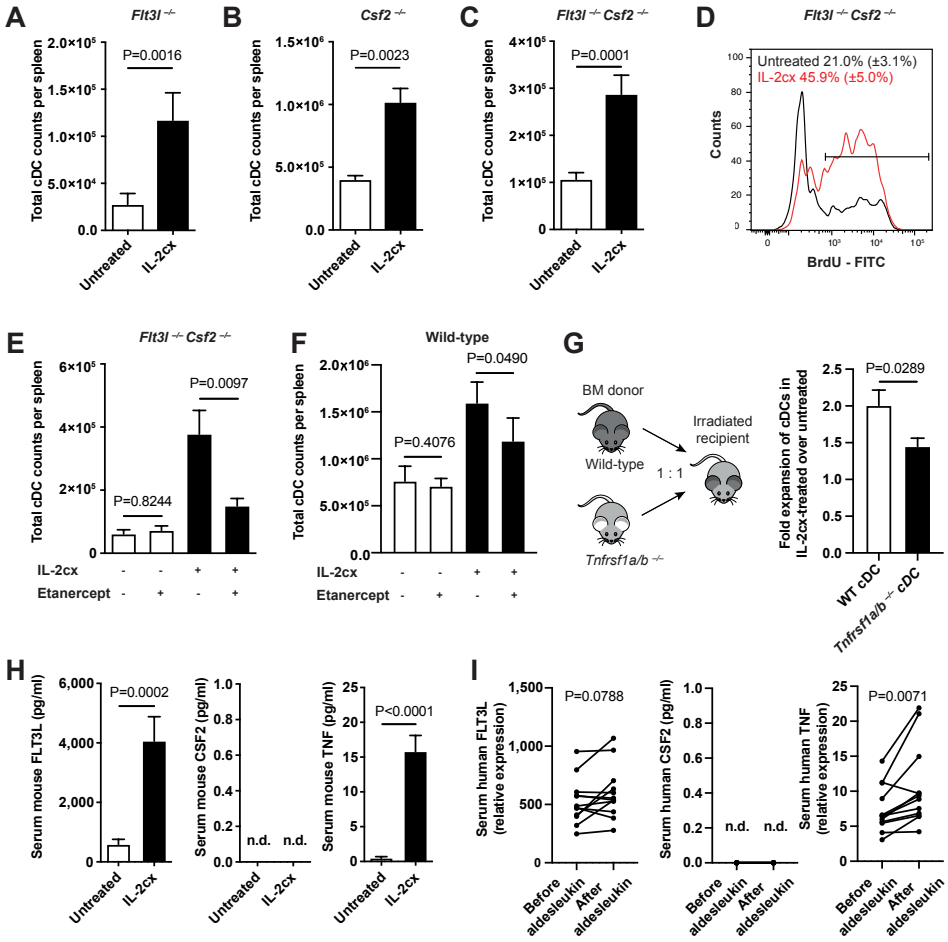
A
Flt3l −/−
Total cDC counts per spleen
P=0.0016
Untreated
IL-2cx
B
Csf2 −/−
P=0.0023
C
Flt3l −/− Csf2 −/−
P=0.0001
D
Flt3l −/− Csf2 −/−
Untreated 21.0% (±3.1%)
IL-2cx 45.9% (±5.0%)
Counts
BrdU - FITC
E
Flt3l −/− Csf2 −/−
P=0.0097
P=0.8244
IL-2cx
Etanercept
F
Wild-type
P=0.0490
P=0.4076
G
BM donor
Wild-type
Tnfrsf1a/b −/−
Irradiated recipient
1 : 1
Fold expansion of cDCs in IL-2cx-treated over untreated
P=0.0289
WT cDC
Tnfrsf1a/b −/− cDC
H
Serum mouse FLT3L (pg/ml)
P=0.0002
Serum mouse CSF2 (pg/ml)
n.d.
Serum mouse TNF (pg/ml)
P<0.0001
I
Serum human FLT3L (relative expression)
P=0.0788
Serum human CSF2 (pg/ml)
Serum human TNF (relative expression)
P=0.0071
Before aldesleukin
After aldesleukin

Figure 4

Fig. 4. IL-2 immunotherapy induces production of several DC mitogens.

(A to **C)** Total splenic cDC counts from *Flt3l*$^{-/-}$ (*n* = 9 to 11 mice from *N* = 4 independent experiments) (A), *Csf2*$^{-/-}$ (*n* = 4 to 6 mice from *N* = 2 independent experiments) (B), or *Flt3l*$^{-/-}$ *Csf2*$^{-/-}$ (*n* = 20 mice per group from *N* = 5 independent experiments) (C) mice treated with IL-2cx. Data are presented as mean +/- SEM. (**D**) Proliferation of cDCs in *Flt3l*$^{-/-}$ *Csf2*$^{-/-}$ mice shown by BrdU incorporation over 3 days. Data are presented as mean +/- SEM (*n* = 14 mice from *N* = 3 independent experiments). Line indicates region quantified. (**E** and **F**) Total splenic cDC counts in *Flt3l*$^{-/-}$ *Csf2*$^{-/-}$ (*n* = 5 to 6 mice per group from *N* = 3 independent experiments) (E) or WT (*n* = 9 mice per group from *N* = 3 independent experiments) (F) mice receiving indicated treatments. Data are presented as mean +/- SEM. (**G**) Expansion of WT and *Tnfrsf1a/b*$^{-/-}$ cDCs following IL-2cx treatment of mice previously irradiated lethally and reconstituted with a 1:1-mix of bone marrow cells from the indicated donor mice. Data are presented as mean +/- SEM (*n* = 12 mice per group from *N* = 4 independent experiments). (**H**) Measurement of mouse FLT3L, CSF2, and TNF in serum using enzyme-linked immunosorbent assay (ELISA). Data are presented as mean +/- SEM (*n* = 6 to 11 mice per group from *N* = 3 independent experiments). (**I**) Measurements of human FLT3L and TNF using proximity extension assay and CSF2 using ELISA in sera of patients before and after receiving aldesleukin as described in Fig. 1F (*n* = 10 to 12 individual patients). *P*-values were calculated using Mann-Whitney test (A), unpaired t-tests (B, C, G and H), repeated measure one-way ANOVA with Holm-Sidak correction for multiple comparison (E), mixed-effects model with Holm-Sidak correction for multiple comparison (F), or paired t-test (I). n.d., not detectable.

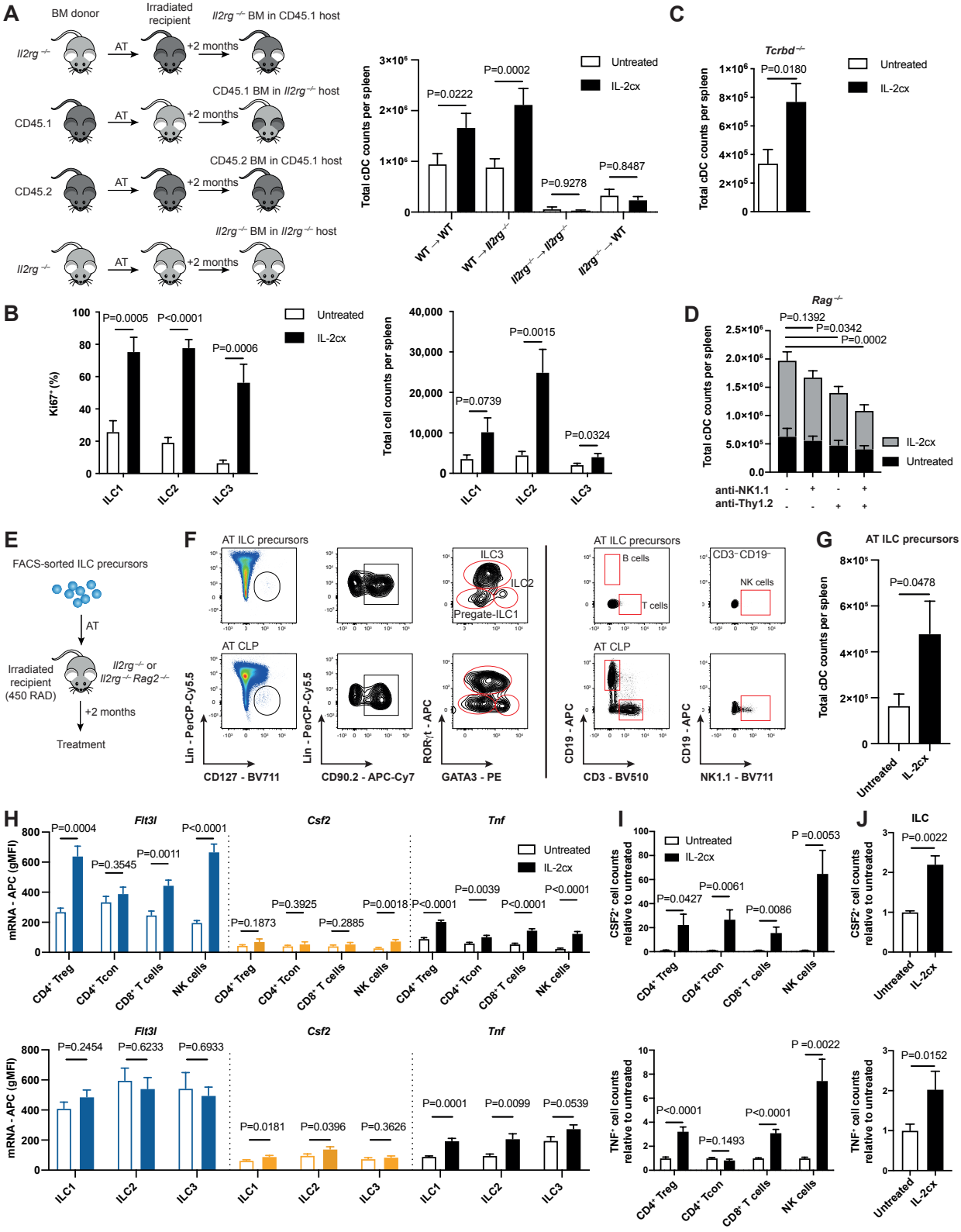
A
BM donor
Irradiated recipient
Il2rg−/− BM in CD45.1 host
Il2rg−/−
AT
+2 months
CD45.1
CD45.1 BM in Il2rg−/− host
CD45.2
CD45.2 BM in CD45.1 host
Il2rg−/− BM in Il2rg−/− host
Total cDC counts per spleen
Untreated
IL-2cx
P=0.0222
P=0.0002
P=0.9278
P=0.8487
WT → WT
WT → Il2rg−/−
Il2rg−/− → Il2rg−/−
Il2rg−/− → WT
C
Tcrbd−/−
P=0.0180
B
Ki67+ (%)
P=0.0005
P<0.0001
P=0.0006
ILC1
ILC2
ILC3
Total cell counts per spleen
P=0.0739
P=0.0015
P=0.0324
D
Rag−/−
P=0.1392
P=0.0342
P=0.0002
anti-NK1.1
anti-Thy1.2
E
FACS-sorted ILC precursors
Irradiated recipient (450 RAD)
Il2rg−/− or Il2rg−/− Rag2−/−
Treatment
F
AT ILC precursors
AT CLP
ILC3
ILC2
Pregate-ILC1
B cells
T cells
CD3− CD19−
NK cells
Lin - PerCP-Cy5.5
CD127 - BV711
CD90.2 - APC-Cy7
RORγt - APC
GATA3 - PE
CD19 - APC
CD3 - BV510
NK1.1 - BV711
G
AT ILC precursors
P=0.0478
H
Flt3l
Csf2
Tnf
mRNA - APC (gMFI)
P=0.0004
P=0.3545
P=0.0011
P<0.0001
P=0.1873
P=0.3925
P=0.2885
P=0.0018
P<0.0001
P=0.0039
P<0.0001
P<0.0001
CD4+ Treg
CD4+ Tcon
CD8+ T cells
NK cells
P=0.2454
P=0.6233
P=0.6933
P=0.0181
P=0.0396
P=0.3626
P=0.0001
P=0.0099
P=0.0539
I
CSF2+ cell counts relative to untreated
P=0.0427
P=0.0061
P=0.0086
P =0.0053
TNF+ cell counts relative to untreated
P<0.0001
P=0.1493
P<0.0001
P =0.0022
J
ILC
P=0.0022
P=0.0152

Figure 5

Fig. 5. IL-2–stimulated innate and adaptive lymphoid cells produce DC-active cytokines.

(**A**) Mice with chimeric bone marrow (BM) were generated by adoptive transfer (AT) of either *Il2rg*$^{-/-}$, CD45.1 wild-type (WT), or CD45.2 WT lineage-depleted BM cells into lethally-irradiated *Il2rg*$^{-/-}$ or CD45.1 hosts. Two months later mice were treated as indicated. Data are presented as mean +/- SEM (n = 4 to 11 mice per group from N = 2 to 4 independent experiments). (**B**) Ki67^{+} proliferating splenic innate lymphoid cells (ILC, left panel) and total ILC counts (right panel) upon IL-2cx treatment. ILCs were defined as Lin (CD3, CD5, CD8, CD11b, CD11c, CD19, B220, Ter119)$^{-}$ CD127^{+} CD90^{+}; with ILC1 defined as TBET^{+}, ILC2 as GATA3^{+}, and ILC3 as RORγt^{+} (fig. S5E). Data are presented as mean +/- SEM (n = 8 to 14 mice per group from N = 3 to 5 independent experiments). (**C**) Expansion of splenic cDCs in *Tcrbd*$^{-/-}$ mice after treatment with IL-2cx. Data are presented as mean +/- SEM (n = 10 to 13 mice per group from N = 4 independent experiments). (**D**) Expansion of splenic cDCs upon IL-2cx treatment in *Rag*$^{-/-}$ mice additionally depleted of NK cells, ILCs, or both. NK cells were depleted by injection of anti-NK1.1 monoclonal antibody; ILCs were depleted by injection of anti-CD90.2 monoclonal antibody. Data are presented as mean +/- SEM (n = 6 to 9 mice per group from N = 3 to 4 independent experiments). (**E** to **G**) Diagram of experimental setup: ILC precursors or control common lymphoid progenitor (CLP) cells were purified with fluorescence-activated cell sorting (FACS) before adoptive transfer into sublethally-irradiated *Il2rg*$^{-/-}$ or *Il2rg*$^{-/-}$ *Rag2*$^{-/-}$ recipient mice (E). Two months later, immune cell populations reconstituted from ILC precursors (AT ILC, upper panel) and CLP (AT CLP, lower panel) were analyzed to verify successful engraftment (F). Mice reconstituted with

ILC precursors were subsequently treated as indicated and splenic cDCs were quantified (G). Data are presented as mean +/- SEM (n = 6 to 7 mice per group from N = 3 independent experiments). (**H**) Flow cytometry-based RNA assay showing expression of *Flt3l*, *Csf2*, and *Tnf* mRNA geometric mean-fluorescence intensity (gMFI) in $CD4^+$ regulatory T (Treg), $CD4^+$ conventional T (Tcon), $CD8^+$ T, natural killer (NK) cells, ILC1, ILC2, and ILC3. Data are presented as mean +/- SEM (n = 6 mice per group from N = 2 independent experiments). (**I** and **J**) Counts of indicated immune cell subsets producing CSF2 (upper graphs) or TNF (lower graphs) in mice treated with IL-2cx or left untreated (n = 8 to 10 mice per group from N = 2 to 3 independent experiments) (I), and ILCs (n = 6 mice per group from N = 3 independent experiments) (J). Data are presented as mean values +/- SEM. Statistical significance was tested with Mann-Whitney test (A), multiple t-tests (B, H, and I), unpaired t-test (C, G, and J), or one-way ANOVA with Holm-Sidak correction for multiple comparison (D).

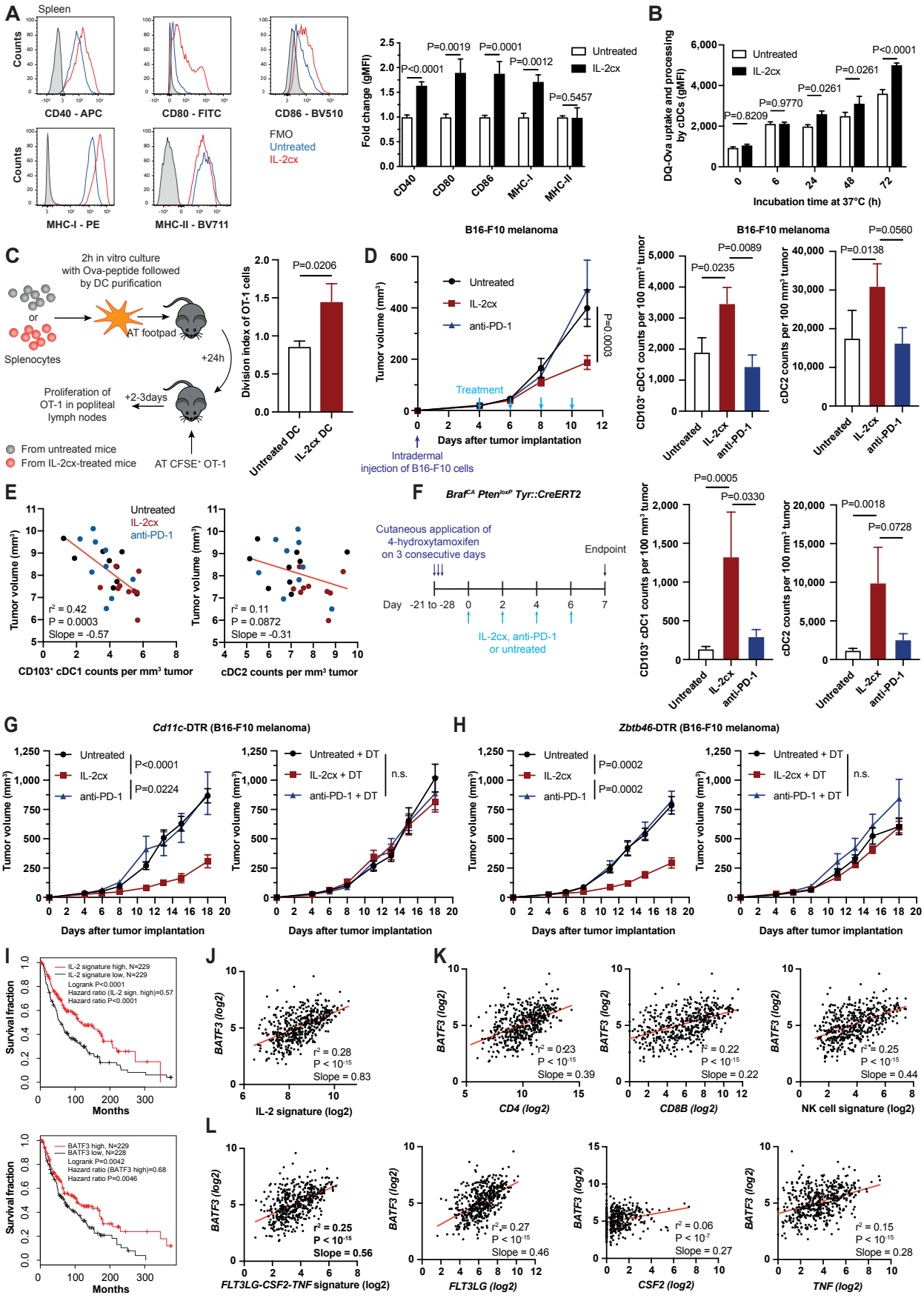
A
Spleen
Counts
CD40 - APC
CD80 - FITC
CD86 - BV510
MHC-I - PE
MHC-II - BV711
FMO
Untreated
IL-2cx
Fold change (gMFI)
P<0.0001
P=0.0019
P=0.0001
P=0.0012
P=0.5457
CD40
CD80
CD86
MHC-I
MHC-II
B
DQ-Ova uptake and processing by cDCs (gMFI)
P=0.8209
P=0.9770
P=0.0261
P=0.0261
P<0.0001
Incubation time at 37°C (h)
C
2h in vitro culture with Ova-peptide followed by DC purification
or
Splenocytes
AT footpad
+24h
Proliferation of OT-1 in popliteal lymph nodes
+2-3days
From untreated mice
From IL-2cx-treated mice
AT CFSE+ OT-1
Division index of OT-1 cells
P=0.0206
Untreated DC
IL-2cx DC
D
B16-F10 melanoma
Tumor volume (mm³)
Untreated
IL-2cx
anti-PD-1
P=0.0003
Treatment
Days after tumor implantation
Intradermal injection of B16-F10 cells
B16-F10 melanoma
CD103+ cDC1 counts per 100 mm³ tumor
cDC2 counts per 100 mm³ tumor
P=0.0089
P=0.0235
P=0.0560
P=0.0138
E
Tumor volume (mm³)
Untreated
IL-2cx
anti-PD-1
r² = 0.42
P = 0.0003
Slope = -0.57
CD103+ cDC1 counts per mm³ tumor
r² = 0.11
P = 0.0872
Slope = -0.31
cDC2 counts per mm³ tumor
F
BrafCA PtenloxP Tyr::CreERT2
Cutaneous application of 4-hydroxytamoxifen on 3 consecutive days
Endpoint
Day -21 to -28 0 2 4 6 7
IL-2cx, anti-PD-1 or untreated
CD103+ cDC1 counts per 100 mm³ tumor
cDC2 counts per 100 mm³ tumor
P=0.0005
P=0.0330
P=0.0018
P=0.0728
G
Cd11c-DTR (B16-F10 melanoma)
Tumor volume (mm³)
Untreated
IL-2cx
anti-PD-1
P<0.0001
P=0.0224
Untreated + DT
IL-2cx + DT
anti-PD-1 + DT
n.s.
Days after tumor implantation
H
Zbtb46-DTR (B16-F10 melanoma)
P=0.0002
P=0.0002
I
IL-2 signature high, N=229
IL-2 signature low, N=229
Logrank P<0.0001
Hazard ratio (IL-2 sign. high)=0.57
Hazard ratio P<0.0001
Survival fraction
Months
BATF3 high, N=229
BATF3 low, N=228
Logrank P=0.0042
Hazard ratio (BATF3 high)=0.68
Hazard ratio P=0.0046
J
BATF3 (log2)
r² = 0.28
P < 10⁻¹⁵
Slope = 0.83
IL-2 signature (log2)
K
r² = 0.23
P < 10⁻¹⁵
Slope = 0.39
CD4 (log2)
r² = 0.22
P < 10⁻¹⁵
Slope = 0.22
CD8B (log2)
r² = 0.25
P < 10⁻¹⁵
Slope = 0.44
NK cell signature (log2)
L
r² = 0.25
P < 10⁻¹⁵
Slope = 0.56
FLT3LG-CSF2-TNF signature (log2)
r² = 0.27
P < 10⁻¹⁵
Slope = 0.46
FLT3LG (log2)
r² = 0.06
P < 10⁻⁷
Slope = 0.27
CSF2 (log2)
r² = 0.15
P < 10⁻¹⁵
Slope = 0.28
TNF (log2)

Figure 6

Fig. 6. IL-2 immunotherapy-activated cDCs facilitate anti-tumor responses in mouse and human.

(**A**) Abundance of CD40, CD80, CD86, MHC-I, and MHC-II on splenic cDCs of untreated and IL-2cx-treated mice displayed as representative histograms (left panel) and fold change of gMFI normalized to untreated (right panel). Data are presented as mean +/- SEM (n = 9 mice per group from N = 4 independent experiments). (**B**) Measurement of antigen uptake and processing by cDCs isolated from untreated and IL-2cx-treated mice after 6, 24, 48, and 72 hours. Data are presented as mean +/- SEM (n = 9 mice per group from N = 5 independent experiments). (**C**) Diagram of experimental setup (left): Ovalbumin peptide-loaded, purified cDCs were injected into the footpad of naïve mice; after 24 hours, CFSE-labeled OT-1 cells were adoptively transferred. Two to 3 days later, popliteal lymph nodes were removed and OT-1 cell proliferation was quantified (right panel). Data are presented as mean +/- SEM (n = 11 to 12 mice per group from N = 5 independent experiments). (**D**) Tumor growth kinetics (left) and quantification of tumor-infiltrating cDCs (day 11) (middle and right) in B16-F10 melanoma-bearing mice treated with IL-2cx or anti-PD-1, or left untreated. Treatment was initiated when tumors were visible and palpable and applied every other day (see also fig. S6B, upper panel). Data are presented as mean +/- SEM (n = 9 mice per group from N = 3 independent experiments. For tumor volume data, P-value for IL-2cx compared to untreated is indicated. (**E**) Correlation of cDC1 and cDC2 with tumor volume of tumor-bearing mice on day 11 from same samples as in (D). (**F**) Diagram of experimental paradigm (left). (Right) Quantification of tumor-infiltrating cDCs in *Braf*^{CA} *Pten*^{loxP} *Tyr::CreERT2* mice harboring 4-hydroxytamoxifen-induced tumors. Treatment was started once tumors were visible and palpable. Data are presented as mean +/- SEM (n

= 12 to 14 mice per group from *N* = 2 to 3 independent experiments). (**G** and **H**) Tumor growth kinetics in *Cd11c*-DTR (*n* = 9 to 10 mice per group from 3 independent experiments) (G) and *Zbtb46*-DTR (*n* = 9 to 10 mice per group from 3 independent experiments) (H) BM chimeric mice harboring B16-F10 melanoma. Treatment with IL-2cx and anti-PD-1 was initiated 4 days after tumor cell injection when tumors were visible and palpable and applied 3× weekly for the duration of the experiment. To deplete DCs, diphtheria toxin (DT) was applied 3× weekly starting 1 day before tumor inoculation and for the duration of the experiment (see also fig. S6B, lower panel). Data are presented as mean +/- SEM. (**I**) Survival analysis of patients with cutaneous melanoma according to IL-2 signature and *BATF3* expression (cut-off at 50%). (**J** to **L**) Correlation of *BATF3* with IL-2 signature (J), with *CD4* and *CD8B* expression, with NK cell signature (K), and with *FLT3LG-CSF2-TNF* expression signature (L). Data were retrieved from TCGA (*n* = 473 individual patients). Statistical significance was tested with Mann-Whitney test (A), two-way ANOVA with Holm-Sidak correction for multiple comparison (B and D, left panel), unpaired t-test (C), one-way ANOVA with Holm-Sidak correction for multiple comparison (D, middle graph cDC1), Kruskall-Wallis test with Dunn's multiple comparison test (D, right graph cDC2, and F), Pearson correlation coefficients (E, and J to L), Mixed-effects model with Holm-Sidak correction for multiple comparison (G to H), and Logrank test (I).